2

Underwater acoustic wave propagation

The first aspect of underwater acoustics investigated here is related to the propagation of acoustic waves in water: how can a signal travel from one point to another? And what are the constraints and transformations it undergoes by so doing? The chapter will start with reminders about the fundamental notions associated with the physical nature of acoustic waves, their properties and orders of magnitude, and their practical use and notation; in particular, the *logarithmic notation* (in *decibels*) universally used in acoustics is explained. The main effect of propagation is to decrease the signal amplitude, by *geometrical spreading* on the one part and by *absorption* on the other; the latter is linked to the chemical properties of sea water, and is a definite factor in the propagation of underwater acoustic waves, limiting reachable range at high frequencies. The estimation of *propagation losses* is a paramount factor in the evaluation of sonar system performances. As the underwater propagation medium is limited by two well-marked interfaces (the bottom and the sea surface), the propagation of a signal is often accompanied by a series of *multiple paths* generated by unwanted reflections at these two interfaces. Practically, these multiple echoes show up as bursts, or series, of replicas of the signal transmitted (at high frequencies), or as a spatial field of stable interferences (at low frequencies). Both are common sources of trouble for the reception and exploitation of useful signals. Furthermore, the velocity of acoustic waves varies spatially in the ocean, mostly with depth, because of temperature and pressure constraints. The paths of sound waves are thus *refracted*, depending on the velocity variations encountered, which of course complicates the modeling and interpretation of the sound field spatial structure. The easiest and most efficient modeling technique is known as *geometrical acoustics*, relating the local values of wave propagation direction and velocity (e.g. through the well-known *Snell-Descartes law*). The fundamental principles of geometrical acoustics will be provided here, with the main formulas yielding the ray paths description, travel times and losses along these trajectories. The ease of use of this approach and its very intuitive physical description make it the most popular method in underwater acoustic propagation

modeling. Using this model, we shall introduce a few archetypal propagation configurations, corresponding to simple but typical variations in sound velocity. The wave methods, such as *normal modes* or *parabolic equation*, are theoretically more rigorous than the geometrical approach: they aim at solving directly the equation of wave propagation in a medium with non-constant velocity. At the end of the chapter we shall introduce the fundamental principles of those approaches, whose application is less straightforward than the geometrical, and whose operation is mostly useful for very low frequency stable signals.

This chapter cannot pretend to cover such a wide realm in details, and is restricted to elementary notions. The interested reader should refer to fundamental books (e.g. for general acoustics, Pierce, 1989; Bruneau, 2005; and for underwater acoustic propagation Brekhovskikh and Lysanov, 1992; Medwin and Clay, 1998; Jensen *et al.*, 1994), and, for a deeper insight, to the many articles published along the past half-century.

2.1 ACOUSTIC WAVES

2.1.1 Acoustic pressure

Acoustic waves originate from the propagation of a *mechanical perturbation*. Local compressions and dilations are passed on from one point to the surrounding points, because of the elastic properties of the propagation medium. From one point to the next (for the sake of simplicity, Figure 2.1 and the formulas below illustrate a one-dimension case), this perturbation will propagate away from its source. The propagation rate of this medium perturbation is named *sound speed* or *velocity*.

The same event will be observed at different points in the medium at different instants. If the propagation only occurs along one spatial dimension x (as in Figure 2.1), one can write for a perturbation $s(x, t)$ the conditions:

$$s(x_1, t_1) = s(x_2, t_2) = s(x_3, t_3) = \cdots = s(x_n, t_n) \tag{2.1}$$

The observation times $t_1, t_2, \ldots, t_n$ are linked to the locations $x_1, x_2, \ldots, x_n$ and to the *propagation speed* c by:

$$\begin{cases} x_2 - x_1 = c(t_2 - t_1) \\ x_3 - x_2 = c(t_3 - t_2) \\ \cdots \\ x_n - x_{n-1} = c(t_n - t_{n-1}) \end{cases} \tag{2.2}$$

An acoustic wave requires an *elastic material* support to propagate (i.e. gas, liquid or solid). The mechanical properties of this supporting medium dictate the local value of the sound speed.

The acoustic wave is characterized by the local motion amplitude of each particle in the propagation medium around its position of equilibrium; by the *fluid velocity* corresponding to this motion (this local speed is not to be confused with the

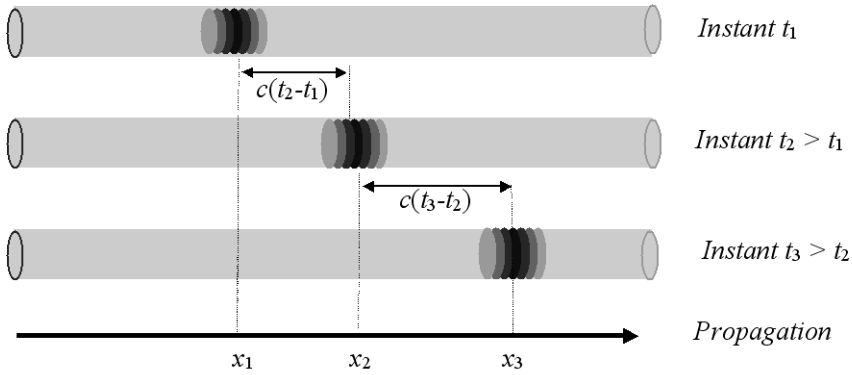

Figure 2.1 One-dimensional propagation of a localized overpressure in a cylindrical waveguide, as a function of time.

wave propagation velocity c); and by the resulting *acoustic pressure*, which is the variation, around the average hydrostatic pressure, caused by the local compressions-dilations imposed by the particular motion. Practically, acoustic pressure is the most often used quantity in underwater acoustics. *Hydrophones* (marine equivalents of aerial microphones), used as underwater sound receivers, are pressure sensors.

The acoustic pressure is expressed in *Pascals* (Pa) or better in *microPascals* (μPa); see Appendix 1.1 for S.I. units definitions. The difference between the acoustic pressure maximal and minimal values, or *dynamics*, may be extremely high in underwater acoustics. Background noise measured in a narrow frequency band under quiet conditions may be only a few tens of microPascals (μPa), whereas the sound level close to a high-power source may reach 10^{12} μPa (i.e. more than 10 orders of magnitude higher!). This justifies using *logarithmic notation* (Section 2.2).

2.1.2 Velocity and density

The propagation velocity of an acoustic wave is determined by the local propagation medium characteristics: the *density* ρ and the *elasticity modulus*[1] E (or, for a fluid, its inverse quantity the *compressibility* χ):

$$c = \sqrt{\frac{E}{\rho}} = \sqrt{\frac{1}{\chi\rho}} \tag{2.3}$$

In sea water, the acoustic wave velocity is close to $c = 1500\,\text{m/s}$ (actually between typically 1450 m/s and 1550 m/s, depending on pressure, salinity and temperature).

[1] The *elasticity modulus E*, or its inverse quantity the *compressibility* χ, quantifies the relative variation of volume (V) or density (ρ) due to pressure (P) variations: $E = \frac{1}{\chi} = \left[-\frac{1}{V}\frac{\partial V}{\partial P}\right]^{-1} = \left[\frac{1}{\rho}\frac{\partial \rho}{\partial P}\right]^{-1}$. This modulus should not be confused with the *Young elasticity modulus* which links deformation and stress in solid media.

The sea water *density* is approximately $\rho = 1{,}030\,\mathrm{kg\,m^{-3}}$ on the average, depending on the same physical parameters.

In a marine sediment (often considered as a fluid medium, as a first approximation), the density ranges between 1,200 and $2{,}000\,\mathrm{kg\,m^{-3}}$. In a water-saturated sediment (where velocity is proportional to the interstitial water sound speed), the sound velocity ranges typically between 1,500–2,000 m/s.

Remember that in air the respective values of sound velocity and density are approximately 340 m/s and $1.3\,\mathrm{kg\,m^{-3}}$.

2.1.3 Frequency and wavelength

Useful acoustic signals are generally not instantaneous perturbations, but maintained *vibrations*. They are characterized by their frequency f (the number of elementary vibrations per second, equivalently expressed in *Hertz* – noted Hz, or in *cycles per second* – noted cps) or by their *period* T (duration of an elementary vibration cycle, linked to frequency by the relation $T = 1/f$). The frequencies used in underwater acoustics range roughly from 10 Hz to 1 MHz, depending on the application[2] (i.e. periods of 0.1 s to 1 μs).

The *wavelength* is the spatial correspondent to time periodicity. It is the elementary spacing between two points in the medium, undergoing the same vibration state with a delay of T, or phase shift of 2π. Stated differently, this is the distance traveled by the wave during one period of the signal with velocity c. It verifies therefore:

$$\lambda = cT = \frac{c}{f} \tag{2.4}$$

For a sound velocity of 1,500 m/s, underwater acoustic wavelengths will be 150 m at 10 Hz, 1.5 m at 1 kHz, and 0.0015 m at 1 MHz. These very diverse values of frequencies and wavelengths obviously correspond to very different physical processes, both for the wave propagation in water, and for the characteristics of the acoustic system itself. The main constraints on the frequencies usable for a particular application are:

- the sound wave *attenuation* in water, limiting the maximum usable range, and whose effect increases very rapidly with frequency;
- the *dimensions* of the sound sources, which increase at lower frequencies, for a given transmission power;
- the *spatial selectivity* related to the *directivity* of acoustic sources and receivers, improving (for a given transducer size) as frequency increases;
- the *target acoustic response*, depending on frequency; a target will reflect less energy as its dimensions are smaller relative to the acoustic wavelength.

In sonar design, all of these points must be taken into consideration when choosing the frequency for a particular application; this choice will always result from a

[2] Marginal applications below 10 Hz or at several MHz may be encountered.

Table 2.1 Frequency ranges of the main underwater acoustic systems, and indicative order of magnitude of the maximum usable ranges (the latter are not valid for passive sonars, sediment profilers and seismic). Note that some sonar systems can exceed 1 MHz.

Frequency (kHz)	0.1	1	10	100	1000
Maximum ranges (km)	1000	100	10	1	0.1
Multibeam sounders			■	■	
Sidescan sonars				■	■
Transmission and positioning			■	■	
Active military sonars		■	■		■
Passive military sonars	■	■	■		
Fishery echo sounders & sonars				■	■
Doppler current profilers				■	■
Sediment profilers			■		
Seismic exploration	■	■			

compromise. Table 2.1 shows the frequency ranges commonly used for the different types of underwater acoustic systems.

2.1.4 The wave equation and its elementary solutions

Acoustic waves propagating in gases and liquids follow the laws of fluid mechanics (see e.g. Medwin and Clay, 1998). Their propagation is described by the wave equation:

$$\Delta p = \frac{\partial^2 p}{\partial x^2} + \frac{\partial^2 p}{\partial y^2} + \frac{\partial^2 p}{\partial z^2} = \frac{1}{c^2(x,y,z)} \frac{\partial^2 p}{\partial t^2} \tag{2.5}$$

where p is the acoustic pressure of a wave propagating in the space (x, y, z) as a function of time t, and $c(x, y, z)$ is the local sound velocity. Δ is the Laplacian operator. For a sinusoidal wave of frequency f_0, the wave equation becomes the *Helmholtz equation*:

$$\Delta p + k^2(x,y,z)p = 0 \tag{2.6}$$

where $k(x, y, z) = 2\pi f_0/c(x, y, z) = \omega/c(x, y, z)$ is the wave number, $\omega = 2\pi f_0$ being the *pulsation* or *circular frequency*. For a constant velocity $c(x, y, z) = c$ and propagation restricted to one single direction **x**, Equation (2.5) becomes:

$$\frac{\partial^2 p}{\partial x^2} + \frac{\omega^2}{c^2} p = 0 \tag{2.6a}$$

the solution of which is a pressure wave of the type:

$$p(x,t) = p_0 \exp\left(j\omega\left(t - \frac{x}{c}\right)\right) = p_0 \exp(j(\omega t - kx)) \tag{2.7}$$

with a constant amplitude p_0, and a phase depending on a single Cartesian space coordinate x. The constant phase surfaces associated to this wave are planes

orthogonal to direction **x**. This type of wave is therefore called *plane wave*. The expressions of corresponding particle displacement velocity $v(x,t)$ and amplitude $a(x,t)$ are identical, replacing modulus p_0 by respectively v_0 and a_0.

The fluid velocity **v** is related to the acoustic pressure by the equation:

$$\nabla p = -\rho \frac{\partial \mathbf{v}}{\partial t} \tag{2.8}$$

where ρ is the medium density and ∇ is the *spatial gradient* operator (related to the Laplacian by $\Delta = \nabla \cdot \nabla$).

For a plane wave propagating in the **x** direction, equation (2.8) (actually expressing the fundamental relation of dynamics[3]) provides a simple relation between amplitudes of acoustic pressure p_0, fluid speed v_0 and displacement a_0:

$$\frac{\partial p}{\partial x} = -\rho \frac{\partial v}{\partial t} \Rightarrow p_0 = \rho c v_0 = \rho c \omega a_0 \tag{2.9}$$

where $\omega = 2\pi f_0$ (the angular frequency) links the displacement a to its time-derivative the fluid speed v.

The product ρc is named the *characteristic acoustical impedance* of the propagation medium. It relates the acoustic pressure level to the corresponding motion of particles. The SI-related unit for acoustic impedance is the *Rayleigh*.[4] In a high-impedance medium like water ($\rho c \approx 1.5 \times 10^6$ Rayl), a particle movement with a given amplitude will yield an acoustic pressure level much higher than in a low-impedance medium like air ($\rho c \approx 0.4 \times 10^3$ Rayl).

When considering the propagation in the three spatial directions of an isotropic medium, the solution to the wave equation for a point source[5] is a *spherical wave*:

$$p(R,t) = \frac{p_0}{R} \exp\left(j\omega\left(t - \frac{R}{c}\right)\right) = \frac{p_0}{R} \exp(j(\omega t - kR)) \tag{2.10}$$

The space variable considered here is the oblique distance R to the source. The wave fronts are now spheres centered on the source ($R = 0$), and the pressure amplitude in (2.10) decreases in $1/R$, from its value p_0 conventionally considered 1 meter away from the source.

Plane and spherical waves are the two basic tools for modeling the propagation of acoustic waves (Figure 2.2). *Plane waves* are the easiest to handle; they are used when the amplitude can be approximated to a constant, and the wave fronts show a negligible curvature. These conditions are satisfied far enough away from the sound source, for the modeling of *local processes* (e.g. target echoes). *Spherical waves* are descriptive of a field transmitted at short range by a point-like source

[3] Since the pressure gradient ∇p gives the resulting differential force applied on a unit volume of mass ρ, and $\partial \mathbf{v}/\partial t$ is the acceleration value.

[4] In honor of the English physicist John William Strutt, Lord Rayleigh (1842–1919), one of the most famous names of acoustics, and author of *The Theory of Sound*.

[5] For a spatial function that depends only on radial distance R, the Laplacian operator reads $\Delta p = \frac{1}{R}\frac{d^2}{dR^2}(Rp)$. The verification that expression (2.10) satisfies Eq. (2.6) is straightforward.

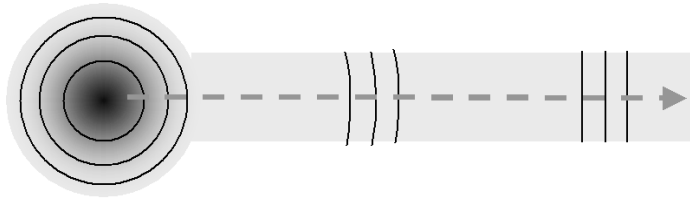

Figure 2.2 Spherical and plane waves: the wave front curvature is an important physical feature close to the source (geometrical structure, amplitude loss), and can be neglected at larger ranges, where the wave may be considered as plane (locally constant amplitude).

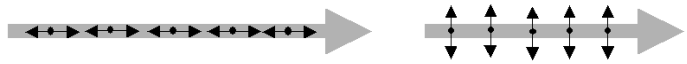

Figure 2.3 Longitudinal (left) and transverse (right) waves: the local motion of the medium (thin arrows) is either parallel or perpendicular to the wave propagation (thick arrows).

(i.e. sufficiently small compared to the wavelength), and when one must account for the amplitude decreasing with propagation from the source.

When the elementary particle motion is parallel to the direction of propagation, the waves are called *pressure waves* (or *longitudinal waves*, or *compressional waves*). They are the only ones to be encountered in fluids (liquids and gases). On the other hand, solid materials can also support *shear waves* (or *transverse waves*), in which displacement and propagation direction are perpendicular. They are characterized by two wave velocity values (longitudinal and transverse), which of course makes the models more complicated (Figure 2.3). In underwater acoustics, most propagation processes can be described by pressure waves. However, transverse waves are to be taken into account when modeling propagation in consolidated sediments and scattering by solid targets.

2.1.5 Intensity and power

The propagation of a sound wave is associated with an *acoustic energy*. This energy can be decomposed into a *kinetic* part (corresponding to particle motion) and a *potential* part (corresponding to the work done by elastic pressure forces).

The *acoustic intensity* I is the energy flux mean value, per unit of surface and time. It equals the *average product of acoustic pressure by fluid velocity* (Pierce, 1989). For a plane wave of amplitude p_0 and root mean square (RMS) value $p_{rms} = p_0/\sqrt{2}$, this yields:

$$I = \frac{p_0^2}{2\rho c} = \frac{p_{rms}^2}{\rho c} \qquad \text{(in Watts/m}^2\text{)} \tag{2.11}$$

The *acoustic power* P received by a surface Σ is the intensity corrected for the surface considered. For a plane wave, this would be:

$$P = I \times \Sigma = \frac{p_0^2 \Sigma}{2\rho c} = \frac{p_{rms}^2 \Sigma}{\rho c} \qquad \text{(in Watts)} \tag{2.12}$$

Like acoustic pressure, intensity and power can vary enormously. A high-power sonar transmitter may deliver an acoustic power of several tens of kilowatts, whereas a submarine in silent mode might radiate only milliwatts.

2.2 LOGARITHMIC NOTATION: DECIBELS AND REFERENCES

2.2.1. The decibel

Because of their huge dynamics, acoustic values like pressure or power are usually quantified on a *logarithmic scale*, and noted in *decibels* (dB). By definition, the decibel corresponds to ten times the base-10 logarithm of the ratio of two powers. For example, $10\log_{10}(P_1/P_2)$ quantifies the ratio in dB between two powers P_1 and P_2, and a 10-dB difference means that P_1 is 10 times higher than P_2.

Defined for power, the decibel can be adapted to other physical values, for example the acoustic pressure. As the power P_i is proportional to the square of pressure p_i^2 (Formula 2.12), the same ratio can be expressed in dB as:

$$10\log\left(\frac{P_1}{P_2}\right) = 10\log\left(\frac{p_1^2}{p_2^2}\right) = 20\log\left(\frac{p_1}{p_2}\right) \tag{2.13}$$

It should therefore be remembered to use $10\log_{10}(X_1/X_2)$ for quantities akin to energies (power, intensity) and $20\log_{10}(x_1/x_2)$ for quantities akin to acoustic pressure.

A difference of 3 dB between two signals will therefore correspond to an energy ratio of about 2, and a pressure amplitude ratio of $\sqrt{2} \approx 1.4$. A 10-dB difference will correspond to an energy ratio of 10, and an amplitude ratio of $\sqrt{10} \approx 3.1$. A 1-dB difference (which one can consider as a practically achievable limit of accuracy for current underwater acoustic measurements) corresponds to around 10% variation of the acoustic pressure. Numerical values in dB are usually truncated at the first decimal digit.

One should also remember that the product of several variables translates into the sum of their values in dB ($[A \times B]_{\mathrm{dB}} = A_{\mathrm{dB}} + B_{\mathrm{dB}}$), due to the properties of logarithmic operations.

Conversely the sum in dB of physical values does not equal the sum of their individual values in dB. Table 2.2 shows the level increase of a signal A when adding (in energy terms, i.e. in $10\log_{10}$) a second signal B, depending on their level differences. For example, if the level of B is larger than the level of A by 5 dB, the level of the sum $A + B$ will be 6.2 dB larger than the level of A alone, and 1.2 dB larger than B alone.

Table 2.2 Correspondence between the level difference (in dB) between two signal intensities A and B, and the level increase obtained by their quadratic summations.

$B_{\mathrm{dB}} - A_{\mathrm{dB}}$	0	1	2	3	4	5	7	10	12	15	20
$[A+B]_{\mathrm{dB}} - A_{\mathrm{dB}}$	3.0	3.5	4.1	4.8	5.5	6.2	7.8	10.4	12.3	15.1	20.0
$[A+B]_{\mathrm{dB}} - B_{\mathrm{dB}}$	3.0	2.5	2.1	1.8	1.5	1.2	0.8	0.4	0.3	0.1	0.0

N.B. In the following, the base-10 logarithm $\log_{10}(A)$ will be simply noted log(A) or log A. When needed, the base-*e* logarithm will be noted ln(A).

2.2.2 Absolute references and levels

A *reference level* is necessary if one is to give absolute pressure or intensity levels in dB. In underwater acoustics, the pressure reference is the microPascal[6] ($p_{ref} = 1\,\mu\text{Pa}$).

Hence an absolute pressure level in dB is to be written as:

$$p_{dB} = 20\log\left(\frac{p}{p_{ref}}\right) \tag{2.14}$$

therefore expressed in dB relative to 1 μPa, noted dB *re* 1 μPa (or dB/1μPa). Clearly, the pressure definition should be the same for p and p_{ref}, and both should be defined for example as RMS values, or as peak-to-peak values.

The dB-scale reference should be explicitly given, since the reference level definition for underwater acoustic pressure may be a source of confusion:

- This absolute pressure reference of 1 μPa is different from the reference in air, which is 20 μPa (average human hearing threshold at 1 kHz). The same absolute pressure level would therefore be expressed as "absolute decibels", with a value higher by $20\log(20) \approx 26$ dB, if considered in water rather than in air (making obvious the need for specifying the reference).
- It should be said that the underwater acoustic reference for pressure has long been the *microbar*, worth 10^5 μPa. Absolute level values in dB *re* 1 μPa are higher by $20\log(10^5) = 100$ dB than those expressed in dB *re* 1 μbar.

For intensity, an often-considered reference is the intensity corresponding to an RMS pressure level of 1 μPa, hence $I_{ref} = 0.67 \times 10^{-18}\,\text{W/m}^2$. Using this reference intensity, the same value in dB is usable for a pressure level and for the intensity level corresponding to the same pressure.

Contrarily, if one wishes to refer intensity to a unity reference value, the relation between values of the signal pressure in dB (*re* 1 μPa) and of its intensity (*re* $1\,\text{W/m}^2$) is readily obtained, using $I = p^2/\rho c$:

$$\begin{aligned} 10\log\left(\frac{I}{1\,\text{W/m}^2}\right) &= 20\log\left(\frac{p_{rms}}{1\,\text{Pa}}\right) + 10\log\left(\frac{1\,\text{Nsm}^{-3}}{\rho c}\right) \\ &= 20\log\left(\frac{p_{rms}}{1\,\mu\text{Pa}}\right) + 20\log\left(\frac{1\,\mu\text{Pa}}{1\,\text{Pa}}\right) - 61.8 \\ &= 20\log\left(\frac{p_{rms}}{1\,\mu\text{Pa}}\right) - 181.8 \end{aligned} \tag{2.15a}$$

[6] Remember that the Pascal (Pa) is the SI-derived unit for pressure; it is defined as $1\,\text{N/m}^2$. See Appendix A.1.1 for unit definition.

A useful relation is between the power radiated by a source and the acoustic pressure at a reference range of 1 m. If the source radiation is spherical, then the surface Σ to consider is 4π, and the radiated power writes, from (2.15a):

$$10\log\left(\frac{P}{1\,\mathrm{W}}\right) = 10\log\left(\frac{I\,\Sigma}{1\,\mathrm{W}}\right) = 10\log\left(\frac{I}{1\,\mathrm{W/m^2}}\right) + 10\log\left(\frac{\Sigma}{1\,\mathrm{m^2}}\right)$$

$$= 20\log\left(\frac{p_{rms}}{1\,\mu\mathrm{Pa}}\right) - 181.8 + 10\log(4\pi) \qquad (2.15b)$$

$$= 20\log\left(\frac{p_{rms}}{1\,\mu\mathrm{Pa}}\right) - 170.8$$

2.3 BASICS OF PROPAGATION LOSSES

When acoustic waves propagate, the most evident effect is their loss of intensity, because of *geometric spreading* (*divergence* effect) and *absorption* of acoustic energy by the propagation medium itself. This *propagation loss* (or *transmission loss*) is a key parameter for acoustic systems, as it constrains the amplitude of the signal received, hence the receiver performance, directly dependent on the signal-to-noise ratio.

2.3.1 Geometric spreading losses

Propagation of an acoustic wave from a sound source spreads the transmitted acoustic energy over a larger and larger surface. As energy is conserved, the intensity will decrease proportionally to the inverse of the surface. This process is known as *geometric spreading loss*.

The simplest (and most useful) case is the homogeneous, infinite medium, with a small-dimension source radiating in all directions (point source). The energy transmitted is conserved, but is spread over spheres of larger and larger radii (Figure 2.4).

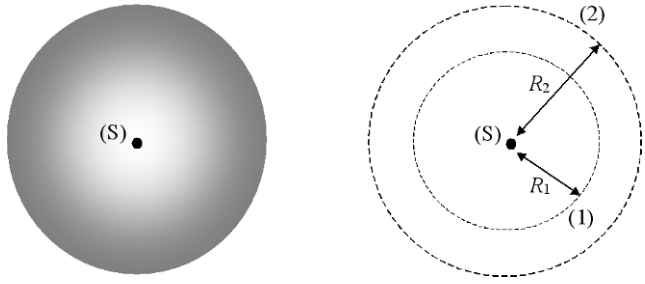

Figure 2.4 Spherical spreading: the acoustic intensity decreases with distance from the source, in inverse proportion to the sphere surface.

The decrease in local acoustic intensity between points (1) and (2) is then inversely proportional to the ratio of the surfaces Σ_1 and Σ_2 of the spheres:

$$\frac{I_2}{I_1} = \frac{\Sigma_1}{\Sigma_2} = \frac{4\pi R_1^2}{4\pi R_2^2} = \left(\frac{R_1}{R_2}\right)^2 \tag{2.16}$$

where R_i are the radial distances from the source. Hence intensity decreases in $1/R^2$, and pressure in $1/R$. This is the amplitude dependence in range already introduced (Section 2.1.4) for spherical waves. The spreading transmission loss, considered from the reference unit distance ($R_{1\mathrm{m}} = 1\,\mathrm{m}$) can be expressed in dB as:

$$TL = 20\log\left(\frac{R}{R_{1\mathrm{m}}}\right) \tag{2.17}$$

Spherical spreading loss is commonly expressed as $TL = 20\log R$, with no reference to the unit distance; although incorrect, this usage[7] is convenient and widespread.

2.3.2 Absorption losses

Sea water is a *dissipative* propagation medium; it absorbs a part of the transmitted wave energy, which is dissipated through viscosity or chemical reactions (thermal conduction being weak in water). The local amplitude decrease is proportional to the amplitude itself; hence the acoustic pressure decreases exponentially with distance. This will add to spreading losses. For example, for a spherical wave, the pressure becomes:

$$p(R,t) = \frac{p_0}{R}\exp(-\gamma R)\exp\left(j\omega\left(t - \frac{R}{c}\right)\right) \tag{2.18}$$

Attenuation is here quantified by the parameter γ (expressed in Neper/m). The exponential decrease of pressure gives a loss in dB proportional to propagation range: this is conveniently expressed through an *attenuation coefficient* α in decibels per meter (dB/m), related to γ by $\alpha = 20\gamma\log e \approx 8.686\gamma$. Note that, practically, attenuation of sound in seawater is best-dimensioned in dB/km.

Absorption is often the most limiting factor in acoustic propagation. Its amount depends strongly on the propagation medium and the frequency. In sea water, absorption comes from:

- *pure water viscosity*, the effect of which increases with squared frequency;
- *relaxation of magnesium sulphate* ($MgSO_4$) molecules below 100 kHz;
- *relaxation of boric acid* ($B(OH)_3$) molecules below 1 kHz.

Molecular relaxation (see e.g. Medwin and Clay, 1998) consists in dissociation of ionic compounds in solution (here $MgSO_4$ and $B(OH)_3$), due to local pressure variations caused by the acoustic wave. This process is dominant for sound

[7] Obviously coming from spoken language habits.

absorption in sea water. If the period of the local pressure variation is longer than the time necessary for the molecule to recompose itself (*relaxation time*), the process is reproduced at every cycle, and dissipates energy permanently. So the attenuation due to this process appears at frequencies *lower* than the characteristic relaxation frequency of the relevant compound.

Ever since the beginnings of underwater acoustics, a high amount of attention has been brought to the modeling of absorption coefficients, and many models have been proposed. The most recent ones are under the form:

$$\alpha = C_1 \frac{f_1 f^2}{f_1^2 + f^2} + C_2 \frac{f_2 f^2}{f_2^2 + f^2} + C_3 f^2 \tag{2.19}$$

The first two terms of this formula show the contributions from the two relaxation processes; the third term corresponds to pure water viscosity. The relaxation frequencies f_i and coefficients C_i depend on temperature, hydrostatic pressure and salinity; they are determined by experiments in laboratory or at sea.

The model mainly[8] used today was proposed by Francois and Garrison (1982a, b). It is detailed hereunder and illustrated in Figure 2.5; it uses explicitly temperature, salinity and hydrostatic pressure, as well as frequency. Based upon a large number of previous experimental results and theoretical studies, it is very complete and accurate; its use is highly recommended.

2.3.2.1 Model of Francois-Garrison

The absorption coefficient is decomposed into three terms, corresponding to the contributions of boric acid, magnesium sulfate and pure water:

$$\alpha = A_1 P_1 \frac{f_1 f^2}{f_1^2 + f^2} + A_2 P_2 \frac{f_2 f^2}{f_2^2 + f^2} + A_3 P_3 f^2 \tag{2.20}$$

where α is the attenuation, in dB/km. z is the depth, in m; S is the salinity, in p.s.u. (practical salinity units, see Section 2.6.1); T is the temperature, in °C; and f is the frequency, in kHz.

The contribution of boric acid $B(OH)_3$ reads:

$$\begin{cases} A_1 = \dfrac{8.86}{c}\, 10^{(0.78\,pH-5)} \\ P_1 = 1 \\ f_1 = 2.8\sqrt{\dfrac{S}{35}}\, 10^{(4-1245/(T+273))} \\ c = 1412 + 3.21T + 1.19S + 0.0167z \end{cases} \tag{2.21}$$

[8] Previous models most often found in the literature are those by Thorp (1967), Leroy (1967), or Fisher and Simmons (1977). The Thorp model is a convenient simplified model for low-frequency sound (below 50 kHz):

$$\alpha = [0.11/(1 + f^2) + 44/(4100 + f^2)]f^2$$

where f is the frequency in kHz.

The contribution of magnesium sulfate $Mg(SO)_4$ reads:

$$\begin{cases} A_2 = 21.44 \dfrac{S}{c}(1 + 0.025T) \\ P_2 = 1 - 1.37 \times 10^{-4} z + 6.2 \times 10^{-9} z^2 \\ f_2 = \dfrac{8.17 \times 10^{(8-1990/(T+273))}}{1 + 0.0018(S-35)} \end{cases} \tag{2.22}$$

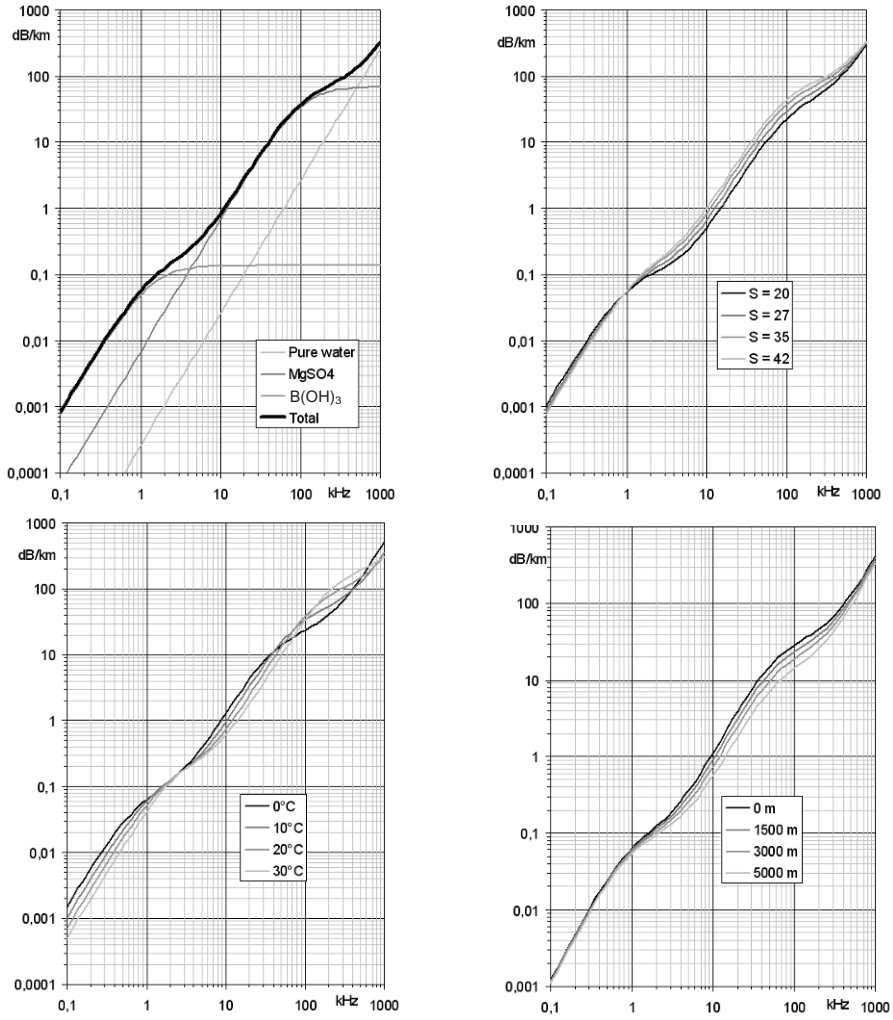

Figure 2.5 Sound absorption coefficient in sea water, as a function of frequency. Top left: contribution of the three components for average conditions ($T = 15°C$, $S = 35$ p.s.u., $z = 0$). Top right: influence of salinity ($T = 15°C$, $z = 0$); Bottom left: influence of temperature ($S = 35$ p.s.u., $z = 0$); Bottom right: influence of depth ($T = 5°C$, $S = 35$ p.s.u.).

The contribution of pure water viscosity reads:

$$\begin{cases} P_3 = 1 - 3.83 \times 10^{-5} z + 4.9 \times 10^{-10} z^2 \\ T < 20^{\circ}\mathrm{C} \Rightarrow A_3 = 4.937 \times 10^{-4} - 2.59 \times 10^{-5} T + 9.11 \times 10^{-7} T^2 - 1.5 \times 10^{-8} T^3 \\ T > 20^{\circ}\mathrm{C} \Rightarrow A_3 = 3.964 \times 10^{-4} - 1.146 \times 10^{-5} T + 1.45 \times 10^{-7} T^2 - 6.5 \times 10^{-10} T^3 \end{cases} \tag{2.23}$$

Figure 2.5 illustrates the influence of the various components and parameters of absorption. It also makes clear that absorption increases very rapidly with frequency, and that the orders of magnitude are highly variable. For frequencies of 1 kHz and less, sound attenuation is below a few hundredths of dB/km, and is therefore not a limiting factor. At 10 kHz, a coefficient of around 1 dB/km precludes ranges of more than tens of kilometers. At 100 kHz, the attenuation coefficient reaches several tens of dB/km and the practical range cannot extend further than 1 km. Underwater systems using frequencies in the MHz range will be limited to ranges below 100 m, with an attenuation of several hundreds of dB/km.

2.3.2.2 Depth-dependence

Depth is another very important factor for the absorption coefficient. It can strongly influence the local performance of a system according to its deployment configuration (e.g., sidescan sonar, or data transmitter). At a lesser degree, it can influence the signal propagation throughout the entire water column (e.g., for bathymetry systems).

If the frequency is high enough that the relaxation effect of $MgSO_4$ is predominant, it is often accurate enough to multiply the absorption coefficient at the surface by the coefficient P_2 of Francois and Garrison's model (Equation 2.22). Table 2.3 gives the evolution of P_2 as a function of depth.

For example, at 100 kHz, if the attenuation is 40 dB/km at the surface of a Mediterranean-type water ($S = 38.5$ p.s.u., $T = 14^{\circ}\mathrm{C}$), it decreases to 30 dB/km at 2000 m depth, and 16 dB/km at 6000 m. These variations of course cause very important differences in the maximum ranges attainable.

For particular applications concerned with the total absorption over the entire water column (e.g., for an echosounder signal, propagating from the ship to the bottom and to the ship again), one should account for the integrated absorption:

$$\hat{\alpha}(H) = \frac{1}{H} \int_0^H \alpha(z) dz \tag{2.24}$$

Table 2.3 Evolution of the depth-correction coefficient P_2 with depth (Francois and Garrison's model).

Z (m)	0	500	1000	1500	2000	2500	3000	3500	4000	4500	5000	5500	6000
P_2	1.00	0.93	0.87	0.81	0.75	0.70	0.64	0.60	0.55	0.51	0.47	0.43	0.40

Table 2.4 Depth dependence of the absorption correction term $A(H)$ in Equation (2.25).

$H(m)$	0	500	1000	1500	2000	2500	3000	3500	4000	4500	5000	5500	6000
$A(H)$	1.00	0.97	0.93	0.90	0.86	0.83	0.79	0.76	0.73	0.69	0.66	0.62	0.59

Using the same P_2-dependence, and neglecting the salinity and temperature variations with depth, the mean coefficient now reads:

$$\hat{\alpha}(H) = \alpha(0)A(H) = \alpha(0)\left[1 - 1.37 \times 10^{-4}\frac{H}{2} + 6.21 \times 10^{-9}\frac{H^2}{3}\right] \qquad (2.25)$$

where $\alpha(0)$ is the absorption value at the surface. The values of $A(H)$ are given in Table 2.4 as a function of height H above the seabed.

Once again, these tables only give orders of magnitude showing the effect of depth on attenuation, and they cannot describe every specific case. For accuracy in practical applications, it is recommended to use complete equations, using the exact temperature and salinity profiles, neglected here.

2.3.3 Conventional propagation loss

Spherical spreading, corrected from attenuation, is systematically used as a first approximation when evaluating the propagation loss and the performance of underwater acoustic systems. In dB, the transmission loss reads:

$$TL = 20\log(R/R_{1\mathrm{m}}) + \alpha R \qquad (2.26)$$

where the reference level is considered at the 1-meter reference range $R_{1\mathrm{m}}$ in a homogeneous non-dissipative medium. However, the common usage is to simplify into the more convenient (although formally incorrect) expression:

$$TL = 20\log R + \alpha R \qquad (2.27)$$

Variations of TL with range and frequency are presented in Figure 2.6.

All systems using the echo backscattered from a target are undergoing propagation losses on the outgoing *and* returning paths; the total loss is therefore:

$$2TL = 40\log R + 2\alpha R \qquad (2.27a)$$

One must pay attention to the units used in Equation (2.27). R is expressed in meters, while α is most often expressed in dB/km, and the units should be converted appropriately.

This simple formula (2.27) is often sufficient to evaluate the performance of underwater acoustic systems. However, some applications require specifically adapted propagation models (geometric rays, normal modes, parabolic approximation). In particular this is necessary when spatial velocity variations induce refraction

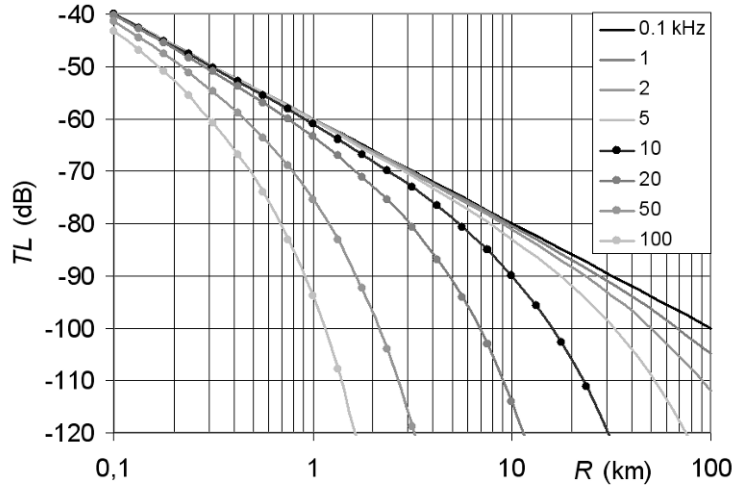

Figure 2.6 Conventional propagation loss $-TL = -20\log R - \alpha R$, as a function of range, for frequencies of 0.1, 1, 2, 5, 10, 20, 50 and 100 kHz respectively. The absorption coefficient α is calculated for environment conditions: $T = 10°\text{C}$, $S = 35$ p.s.u., $z = 10$ m.

of propagation paths, or when the interfaces generate multiple concurrent paths, since geometric spreading cannot then be approximated then by spherical spreading alone.

2.3.4 Effect from air bubbles

Air bubbles in seawater are mainly caused by sea surface movements, but also by the displacement of ship hulls inside the water. They form an inhomogeneous layer, close to the surface, whose dual-phase mixing (water and gas) modifies locally and strongly the acoustic characteristics of the propagation medium (velocity and attenuation). This process decreases in importance as depth increases, because the hydrostatic pressure counteracts the existence of bubbles, and because the air bubble formation processes (waves and hulls) take place close to the sea-surface. Deeper than 10 to 20 m, the effect of surface-generated bubbles can be neglected.

This local perturbation of the propagation medium has severe consequences on performances of hull-mounted sonars:

- additional attenuation, added to sea water absorption, causing the decay of the signals transmitted, and masking the receiving transducers;
- local modification of the sound velocity, causing refraction inside the surface layer;
- parasite backscattered echoes, which can be commonly observed, for example in the first moments of signals recorded by echosounders.

These processes can dramatically impact the performance of an acoustic sensor, possibly making it fail completely, as commonly observed in practice. According to their size and number density, bubbles can simply decrease slightly the levels of echoes, but they can also severely degrade the quality of the measurements, finally inducing detection losses or parasite echoes.

It is of course helpful to control as much as possible the many parameters acting on these performance-limiting processes. The presence of bubble clouds depends for one part on factors linked to the surrounding natural environment, and is therefore uncontrollable (as are weather-induced surface agitation, biological activity, ship's movements, etc.). On the other hand, the hull shape, the speed of the instrument-bearing platform, as well as the position and geometry of the transducers, are important parameters that have to be controlled. In particular, when studying the design and installation of sonar antennas on a hull, special care must be taken that they are placed away from shallow-water streaming areas, potentially loaded with surface-generated bubbles. This is done by studying the hydrodynamic behavior of the hull, through numerical simulations and test tank experiments, and normally leads to the installation of the transducers in the fore part of the hull.

Surface bubbles also modify the reflection characteristics of sound waves at the sea surface, which is masked by an absorbing layer. This extra-attenuation effect needs to be accounted for, when modeling sonar signals propagating along multiple paths and reflecting at the surface.

Many theoretical studies and experimental works have been conducted to investigate air bubbles in water and their acoustic behavior. Each individual bubble acts as a spherical obstacle with a very high acoustic impedance contrast to water, and therefore as a strong scatterer of the incident sound wave. The scattering effect is maximum[9] around the intrinsic resonance frequency of the bubble (see, e.g., Medwin and Clay, 1998):

$$f_R = \frac{3.25}{a}\sqrt{1 + 0.1z} \tag{2.28}$$

where f_R is the resonance frequency (in Hz), z is the depth (in m) and a is the gas sphere radius (in m).

Visco-thermal absorption by the walls of the air bubble adds to the scattering effects. When the bubble population grows, the intensity of the transmitted sound wave is attenuated by the sum of the scattering processes (dominated by the contribution from resonating bubbles) and the absorption processes. The loss in transmitted intensity can then be modeled with a local equivalent absorption coefficient, depending on the individual characteristics of bubbles and their statistical size distribution.

Finally, the acoustical influence of individual bubbles, or the behavior of populations with simple statistical distributions, is well understood theoretically.

[9] The order of magnitude of the extinction (scattering and absorption) cross section of a bubble at resonance frequency is several magnitudes greater than its geometrical cross section πa^2; see Section 3.3.3 in this respect. This explains the importance of bubble clouds on sound propagation

However, this may prove to be of little practical interest, since the problem lies rather in the estimation of the perturbations provoked by evolving, inhomogeneous clouds with hardly predictable bubble populations. Some models are available from the literature; they are generally quite complex, and difficult to summarize here. For a first approach of the impact of shallow bubbles upon surface reflections, one could use the following simple formula (APL, 1994), quantifying the additional loss for a path reflecting on the surface and crossing the entire surface bubble layer:

$$\begin{cases} TL_b = \dfrac{1.26 \times 10^{-3}}{\sin\beta}\, \nu_w^{1.57} f^{0.85} & \text{for } \nu_w \geq 6\,\text{m/s} \\ TL_b = TL_b(\nu_w = 6) e^{1.2(\nu_w - 6)} & \text{for } \nu_w < 6\,\text{m/s}. \end{cases} \tag{2.29}$$

where TL_b (in dB) is the two-way transmission loss caused by bubbles, ν_w (in m/s) is the wind speed 10 m above the surface, f (in kHz) is the signal frequency, and β is the grazing angle. The value of $\nu_w = 6$ m/s corresponds to the threshold for the existence of crashing waves generating bubbles.

Developments in the theory of bubble acoustics can be found in books by Medwin and Clay (1998) or Leighton (1994). For more practical models taking into account the sonar depth, velocity variations and the depth-velocity profile, see, e.g., Hall (1989), or APL (1994).

2.4 MULTIPLE PATHS

2.4.1 Notion of multiple paths

Because the propagation medium is limited by the sea surface and the seabed, the signals, while propagating, undergo successive reflections at the interfaces. Variations in sound velocity within the medium also deform the paths of sound waves. Due to these processes, a given signal can therefore propagate from a source to a receiver along several distinct paths, corresponding to different directions and durations. The main "direct" signal arrives along with a series of echoes, the amplitudes of which decrease with the number of reflections undergone. The time structure of the signal to be processed is of course somewhat affected, and the performance of a system can be highly degraded by these parasite signals, which are most often detrimental, and particularly penalising for data transmission applications. The number of noteworthy multiple paths is highly variable, depending on the configuration; none of them in the best case, up to several tens or even hundreds in long-distance propagation cases (individual paths are then impossible to distinguish inside the multipath structure, and rather show up as a continuous signal trail).

Multiple paths may be considered from two points of view, depending on the sonar type and application. At high frequency, for short signals (shorter than the typical delay between path arrivals), the multipath effect is observable in the time domain, with typical sequences of multiple echoes (Figure 2.7). Whereas, for low-frequency stable signals, the contributions add together permanently; this creates a

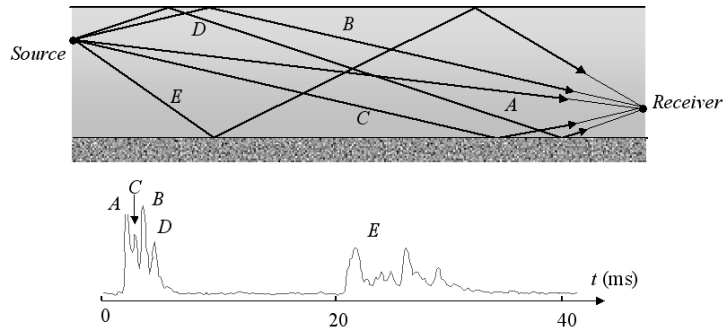

Figure 2.7 Top: multipath trajectories in an isovelocity shallow-water configuration. (*A*) direct path; (*B*) reflection on the surface; (*C*) reflection on the bottom; (*D*) reflection on the surface and bottom; (*E*) reflection on the bottom and surface. Bottom: Multiple paths as visible in the envelope of real time-domain signal. Approximate dimensions: water depth 90 m, horizontal range 1000 m, source depth 15 m, receiver depth 83 m. Note that the first group of 4 arrivals, very clearly distinguishable, spreads over about 4 ms; a second group arrives 20 ms later, with still a very significant intensity, and a more blurred time structure, the individual echoes tending to spread and to merge into a reverberation trail.

stable interference pattern, with strong variations in the field amplitude (a simple case is described in Section 2.4.2).

A dominant and permanent mix of quasi-simultaneous multiple signals raises the phenomenon of *fading*: the interference of multipath arrivals causes strong pseudo-random variations of the resulting sound field amplitude, leading to local deep extinctions at particular frequencies (or points, or instants, depending on the observation configuration). Again, this spatial and frequency-selective effect is especially penalizing for data transmission applications. Its statistical analysis is presented in Chapter 4.

The long delays between multipath arrivals are typical of underwater acoustics; this phenomenon is quite different, in its consequences, from multipaths propagation encountered in electromagnetic propagation, even if they both originate from similar physical processes. The multipaths interference of radio or radar waves mainly cause *fading*, while the echo delays (very short thanks to the speed of light) are usually not troublesome when decoding the received signal. In underwater acoustics, on the contrary, with a low propagation velocity, the multipath time delays create distinguishable echoes and reverberation effects, all lengthening the received signal sequence. Note also that the physical heterogeneity of the waveguide (velocity variations, presence of heterogeneities and scatterers, influence of interfaces) is also much more marked in underwater acoustics than in electromagnetic propagation.

2.4.2 Sea-surface interference

We shall see in Chapter 3 that when a sound wave hits the sea surface (assumed flat) from below, it is reflected with a reflection coefficient $V \approx -1$ (no change in

amplitude, and a phase shift of π). In low-frequency transmission configurations close to horizontal, this perfect reflection yields interesting effects since the surface-reflected signal interferes with the direct-path signal. The coherent summation of the two signals produces spatial *interference fringes*. Noting D the horizontal range (Figure 2.8), and z_s and z_r the respective depths of the source and the receiver, the direct path length reads:

$$R_d = \sqrt{D^2 + (z_s - z_r)^2} \tag{2.30}$$

And the surface-reflected spherical length reads:

$$R_s = \sqrt{D^2 + (z_s + z_r)^2} \tag{2.31}$$

Assuming that z_s and z_r are small relative to D (case of long-range propagation), these expressions can be approximated as:

$$\begin{aligned} R_d &= D\sqrt{1 + \frac{(z_s - z_r)^2}{D^2}} \approx D + \frac{(z_s - z_r)^2}{2D} \\ R_s &\approx D + \frac{(z_s + z_r)^2}{2D} \end{aligned} \tag{2.32}$$

This leads to:

$$R_s \approx R_d + \frac{2z_s z_r}{D} \tag{2.33}$$

Disregarding the amplitude terms (since the spherical ranges R_s and R_d are almost identical for the two paths, so are the propagation losses), and accounting for the sign change of the reflected wave, the field at the receiver is proportional to the sum:

$$\begin{aligned} p &\propto \exp(-jkR_d) - \exp(-jkR_s) \\ &= \exp(-jkR_d)\left[1 - \exp\left(-2jk\frac{z_s z_r}{D}\right)\right] \end{aligned} \tag{2.34}$$

The resulting intensity (disregarding propagation losses) is thus proportional to:

$$|p|^2 \propto 1 - \cos\left(2k\frac{z_s z_r}{D}\right) \tag{2.35}$$

It presents a series of maxima and minima as a function of range. For instance, the minima are given by:

$$2k\frac{z_s z_r}{D} = 2n\pi, \quad \text{with } n = 1, 2, 3 \cdots \Rightarrow D_n = k\frac{z_r z_s}{n\pi} = 2\frac{z_s z_r}{n\lambda} \tag{2.36}$$

The interference nulls get closer in range as n increases. The longest range with a pressure minimum is given by $n = 1$, i.e. $D_1 = 2\frac{z_s z_r}{\lambda}$.

Figure 2.8 shows interference fringe patterns as a function of range and frequency, then range and depth.

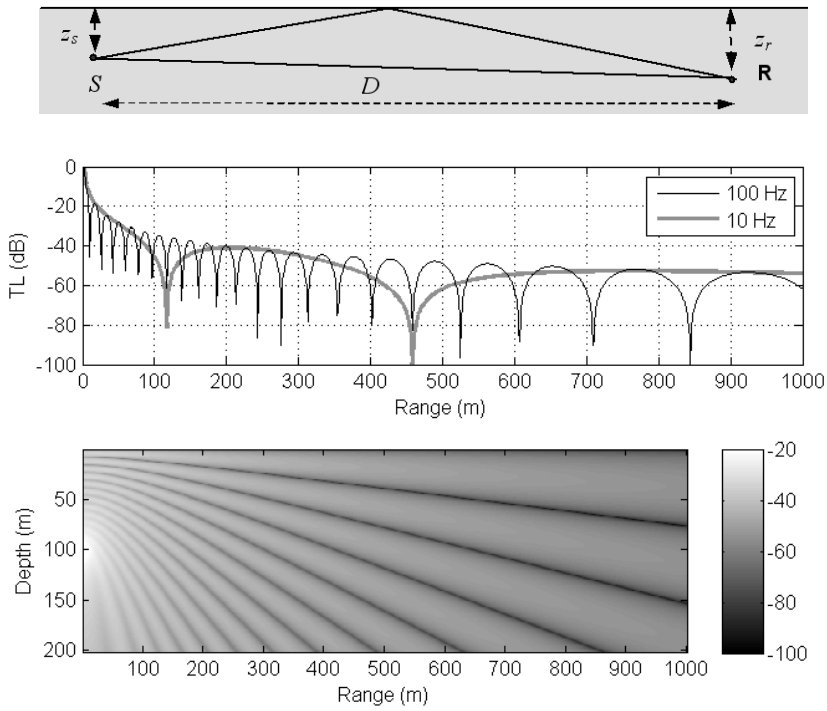

Figure 2.8 Sea-surface interference. Top: geometric configuration; Center: transmission loss as a function of horizontal range, for two frequencies ($f = 10$ and 100 Hz, $z_s = z_r = 200$ m); Bottom: propagation loss in dB, as a function of range and depth ($f = 100$ Hz, $z_s = 100$ m).

2.4.3 An ideal model of multi-path propagation

If the propagation medium is stratified (i.e., the bottom is flat horizontal) and characterized by a constant velocity, the signal transmitted by the source arrives at the receiver by a series of rectilinear paths undergoing multiple reflections on the surface and on the bottom. These different paths correspond to the transmission from *image sources* geometrically obtained by successive symmetries of the actual source relative to the surface and bottom (Figure 2.9).

Image sources are defined by the difference z_{ij} between their ordinates and the ordinate z_r of the receiver. Four kinds of sources are defined, corresponding to different recurrence relations for the successive reflections, and using the water height H and the depths of the transmitter z_t and the receiver z_r:

$$\begin{cases} z_{1i} = 2(i-1)H + z_t - z_r \\ z_{2i} = 2(i-1)H + z_t + z_r \\ z_{3i} = 2iH - z_t - z_r \\ z_{4i} = 2iH - z_t + z_r \qquad \text{with } i = 1, 2, 3 \ldots \end{cases} \tag{2.37}$$

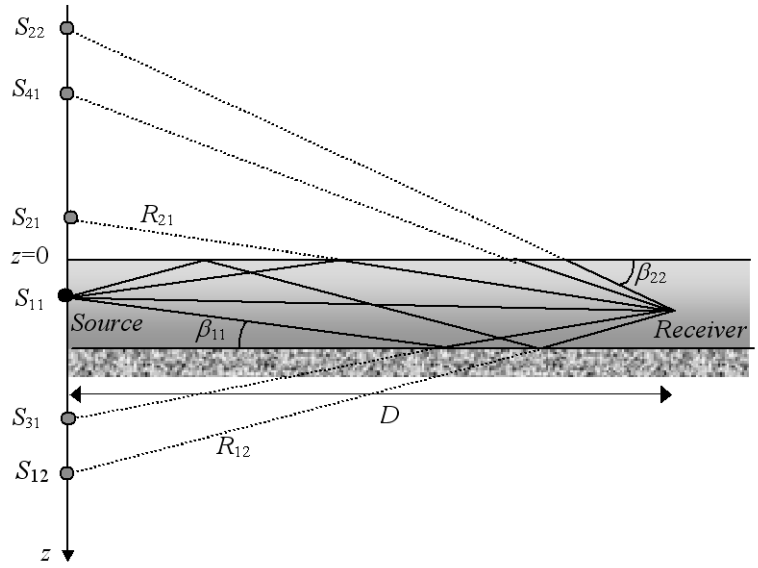

Figure 2.9 Image-sources in a constant-velocity water layer.

The oblique range corresponding to a source ji equals $R_{ji} = \sqrt{z_{ji}^2 + D^2}$, D being the horizontal distance from source to receiver. The grazing angle of the corresponding path is $\beta_{ji} = \arctan(z_{ji}/D)$, and the travel time is $\tau_{ji} = R_{ji}/c$.

The contribution of each image source can be identified with the transmission of a spherical wave, thus with an amplitude decrease in $\exp(-\gamma R)/R$. Losses and phase shifts at the reflections on the surface and at the bottom (for an image-source S_{ji}) are first calculated from the (complex) reflection coefficients of the plane waves $V_s(\beta)$ and $V_b(\beta)$ for $\beta = \beta_{ji}$. The characteristics of these reflection coefficients will be detailed further in Chapter 3. The number of reflections at the surface and at the bottom is a function of the orders i and j:

$$\begin{cases} N_{s_{1i}} = i - 1;\ N_{b_{1i}} = i - 1 \\ N_{s_{2i}} = i;\ N_{b_{2i}} = i - 1 \\ N_{s_{3i}} = i - 1;\ N_{b_{3i}} = i \\ N_{s_{4i}} = i;\ N_{b_{4i}} = i \end{cases} \tag{2.38}$$

If $S(t)$ is the transmitted signal, the contribution of each image source can be written as a delayed replica, affected by its transmission loss and cumulated reflection coefficients:

$$p_{ji}(t) = S(t - \tau_{ji}) \frac{\exp(-\gamma R_{ji})}{R_{ji}} V_s^{N_{sji}}(\beta_{ji}) V_b^{N_{bji}}(\beta_{ji}) = S(t - \tau_{ji}) A_{ji} \tag{2.39}$$

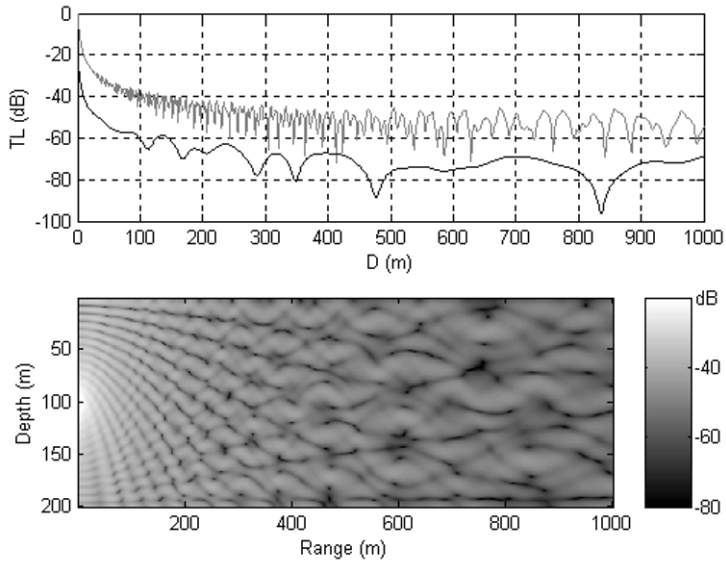

Figure 2.10 Transmission loss TL computed from image sources ($H = 200\,\text{m}$; $z_s = 100\,\text{m}$; $c_2 = 1{,}700\,\text{m/s}$; $\rho_2 = 1{,}800\,\text{kg m}^{-3}$; $\alpha_2 = 0.5\,\text{dB}/\lambda_2$). Top: loss as a function of the range ($z_r = 100\,\text{m}$) for frequencies of 500 Hz and 50 Hz respectively (the latter lowered by 20 dB for the drawing clarity); Bottom: pressure field in dB as a function of range and depth at 100 Hz, to be compared with Figure 2.8.

And the resulting signal is:

$$p(t) = \sum_{i=1,2\ldots} \sum_{j=1}^{4} p_{ji}(t) \tag{2.40}$$

The impulse response of the medium can be written with this model:

$$H(t) = \sum_{i=1,2\ldots} \sum_{j=1}^{4} A_{ji}\delta(t - \tau_{ji}) \tag{2.41}$$

where δ is the Dirac distribution.

This ideal model can be used as a first approximation for shallow water cases, or deep water/small ranges. It yields easy and intuitive formulations of the intensity, time and angular variations of the field, with reasonably accurate results under its validity assumptions (in particular constant velocity); an example of transmission loss is given in Figure 2.10. This model can be used, for example, to simulate signals under multipaths conditions, in order to assess the performance of particular processing techniques.

2.4.4 Average energy flux in a waveguide

In specific configurations of *waveguide propagation*, for example at large ranges in shallow water, the transmitted field is composed of many paths propagating by

successive reflections on the surface and on the bottom. The acoustic energy remains trapped between these two boundaries. If the signal frequency is high enough that the oscillations of the resulting field can be considered as random (and non significant in their detailed small-scale structure), it can be interesting to model the field in terms of *average energy flux*. The principle is to consider, as a function of the cylindrical distance r:

- *spherical propagation* from the source, until the entire channel depth is insonified in a cylindrical mode (see below), hence defining a transition range r_0 (Figure 2.11). This implies the existence of a limit angle, caused either by reflection on the channel boundaries or by refraction effects;
- *cylindrical propagation* from r_0 onwards. Instead of diverging spherically, the acoustic energy spreads on cylindrical surfaces limited by the channel boundaries. Its intensity thus decreases in $10\log(r/r_0)$ (instead of $20\log(R/R_0)$ with spherical propagation).

For instance, in a constant-velocity channel of height H, with a fluid bottom imposing a maximum grazing angle β_0 (see Section 3.1.1), the effective angular sector is defined by the interval $[-\beta_0, +\beta_0]$. Outside this interval, the sound waves quickly become negligible because of the bottom reflection losses. Supposing the source at mid-height, the transition range is obviously defined as (Figure 2.11):

$$r_0 = \frac{H}{2\tan\beta_0} \tag{2.42}$$

The average transmission loss (in dB) then reads:

$$\begin{cases} TL = 20\log r + \alpha r & r < r_0 \\ TL = 20\log r_0 + 10\log\dfrac{r}{r_0} + \alpha r = 10\log(rr_0) + \alpha r & r > r_0 \end{cases} \tag{2.43}$$

Despite its simplicity, this approach is relevant for a quick estimation of the transmission losses under propagation conditions dominated by numerous boundary-reflected multipaths, and when, of course, only the coarse characteristics of the field

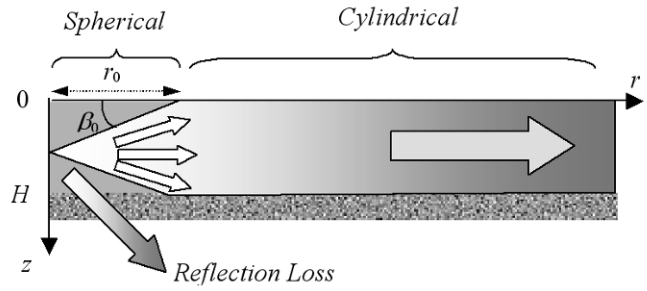

Figure 2.11 The energy flux model: transition at r_0 from spherical to cylindrical.

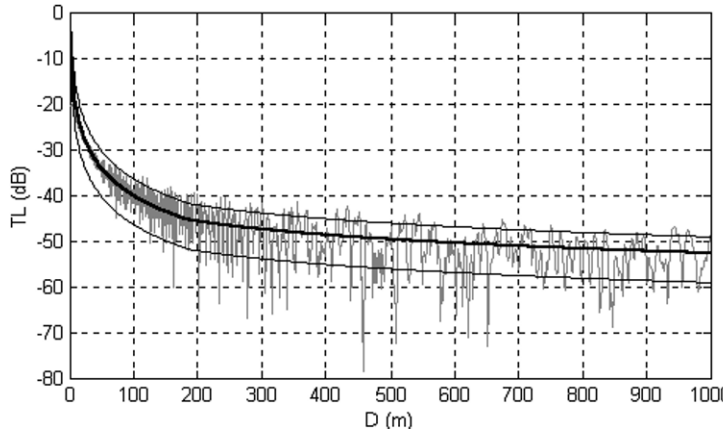

Figure 2.12 Comparison of the average intensity flux (monotonous curves) with a complete computation (image sources in an isovelocity medium, fluctuating curve). The thick line is the average intensity level, the thin ones account for +/− the standard deviation of a Rayleigh amplitude distribution (see Section 4.6.3.2). ($f = 1000$ Hz; $H = 200$ m; $z_0 = 100$ m; $z_r = 100$ m; $c_2 = 1700$ m/s; $R_0 = 187$ m).

are needed. Figure 2.12, for example, presents the acoustic field average intensity decreasing with horizontal range, accounting for the standard deviation of a Rayleigh distribution[10] of pressure amplitude, and compared with a full coherent calculation obtained with the image-sources of Section 2.4.3. As a first approximation, the average energy flux gives a fair estimate of the average field and its fluctuation rate (except, for the latter, at short ranges where the Rayleigh distribution regime for fluctuations is not established yet).

Interestingly, this average intensity concept may be extended to propagation configurations where the sound velocity is not constant, or with slight reflection losses at the boundaries. The transmitted field cannot then any more be taken as a whole, since its features are then angle-dependent: it has to be decomposed into its angular components, and the cyclic characteristics of the various beams must be detailed (see Appendix 2.1 for a more detailed presentation of this approach, which is an intermediate between the average energy flux and geometrical acoustics developed in Section 2.7).

2.4.5 General-case sound field prediction

The elementary idealized solutions presented above (losses in $20 \log R + \alpha R$, image sources, average energy flux) are indeed effective and accurate enough in a number of

[10] See Section 4.6.3.2. The Rayleigh distribution describes the resultant amplitude of a summation of many narrow band signals with the same frequency, random phases and similar amplitudes. Its standard deviation is 0.522 times its mean value. Therefore, these values in dB are $20 \log(1.522) = 3.6$ dB and $20 \log(0.478) = -6.4$ dB.

cases. This should not mask the fact that solving the general-case Helmholtz equation is one of the main theoretical problems in acoustic propagation, and a difficult one. It has motivated researchers for many decades. The complexity of the solutions, and the tools necessary to obtain them, depends on the velocity field structure $c(x, y, z)$, and on the boundary conditions at the propagation medium interfaces (specially the seafloor). The solving techniques change with the frequency range considered:

- At high frequencies, the Helmholtz equation can be approximated by a simpler formula (*eikonal equation*) describing trajectories of acoustic rays (similar to optics); the path of each ray follows the local velocity variations. With this approach, one can follow energy traveling in the waveguide, and reconstruct the field in each point as a sum of multipaths (as a simplification, this is conceptually similar to the source image method, but accounting for path refractions). The time and angle domain characteristics of the signals thus predicted are excellent, and the predictions of energy levels are generally acceptable.
- At low frequencies, one would use *modal field analysis* when the velocity only depends on depth, or the *parabolic equation approximation* when the velocity also depends on horizontal range. In both cases, the monochromatic coherent field is calculated very accurately in each point of the waveguide.

These approaches will be briefly discussed in the rest of this chapter (respectively Sections 2.7 and 2.9), along with some details about the ray-tracing equations, since they are the most used in practice. Much more detailed descriptions can be found in specialist books (e.g., Officer, 1958; Tolstoy and Clay, 1987; Brekhovskikh and Lysanov, 1992; Frisk, 1994; Jensen *et al.*, 1994).

2.5 OTHER DEFORMATIONS OF THE UNDERWATER ACOUSTIC SIGNALS

2.5.1 Doppler effect

The *Doppler effect* is a shift of the apparent signal frequency after propagation, due to a change in the duration of the source-receiver paths during transmission time, caused by the relative displacement of the source and the receiver, or the source and the target.

Let us consider a source transmitting Dirac-like pulses with a regular period T, toward a receiver at distance D. If D does not vary with time, the receiver gets each pulse after a constant time delay $t = D/c$. The period of the signal is therefore not modified, and the apparent frequency remains $f_0 = 1/T$.

Conversely, if D decreases (for example) with time as $D(t) = D - v_r t$, because of the relative speed v_r between the source and the receiver, the time lag between the received pulses will change too.

If the first pulse (transmitted at $t = 0$) arrives at time $t_1 = D(t_1)/c$, the second pulse (transmitted at $t = T$) arrives at time t_2 given by:

$$t_2 = T + \frac{D(t_2)}{c} = T + \frac{D(t_1) - v_r(t_2 - t_1)}{c} \tag{2.44}$$

The time lag between the two successive receptions is then:

$$t_2 - t_1 = \frac{T}{1 + v_r/c} \tag{2.45}$$

hence slightly less than T, since the propagation range has decreased along the transmission time. The apparent frequency of the pulse arrivals is then modified as:

$$f = \frac{1 + \frac{v_r}{c}}{T} = f_0\left(1 + \frac{v_r}{c}\right) \tag{2.46}$$

This frequency variation is the Doppler effect. The frequency shift δf is thus:

$$\delta f = f_0 \frac{v_r}{c} \tag{2.47}$$

where v_r is positive when moving closer, negative when moving away.

For an echo from a target, as the sound travels both ways, the frequency shift comes as:

$$\delta f = 2 f_0 \frac{v_r}{c} \tag{2.48}$$

The Doppler effect complicates the processing of signals, particularly in communication and data transmission applications. But it can be put to good use for some applications. For example, its measurement can be used to determine the speed of a ship relative to the bottom or the water column (*Doppler Velocity Log*, see Section 7.1.3 for details), or to measure the characteristics of a marine current (see Section 7.5.3).

In Anti-Submarine Warfare, the Doppler shift is useful to track a target, and even help to identify it by measuring its speed. Let us consider an acoustic source passing by a fixed receiver (Figure 2.13). The source has a linear speed v, and the minimum range between the source and the receiver is represented by H. With the notations of Figure 2.13, the radial speed component equals:

$$v_r = \frac{-xv}{\sqrt{x^2 + H^2}} \tag{2.49}$$

hence translating, in terms of frequency shift, into:

$$\frac{\delta f}{f_0} = \frac{-xv}{c\sqrt{x^2 + H^2}} \tag{2.50}$$

This last expression shows that the Doppler shift goes to zero and changes sign at the closest point of approach $x = 0$.

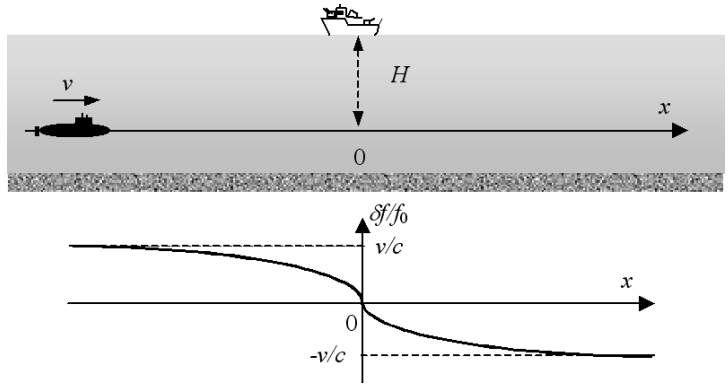

Figure 2.13 Effect of a Doppler shift between a mobile source and a fixed receiver.

The relative frequency variations observed using sonars can be actually significant: $\frac{\delta f}{f_0} \approx 0.7\%$ for a moderate relative speed of 10 knots (18.5 km/h), that is much larger than the typical variations encountered with radar (0.0002% for a plane traveling at 1000 km/h, the radar wave velocity being 3×10^8 m/s).

2.5.2 Time characteristics of echoes

The duration of the transmitted signal strongly influences the shape and the level of the received signals. The concept of *point target* (see Section 3.2.1) assumes the signal is long enough to insonify the target totally at a given time. Long signals allow the maximum intensity of the target response. Conversely, short signals will allow the separation of the different components of the global echo (e.g. to distinguish close targets).

The backscattered signal is lengthened by δt. This lengthening is a function of the apparent length L_a of the target insonified along the propagation direction (Figure 2.14). It reads:

$$\delta t = \frac{2L_a}{c} \tag{2.51}$$

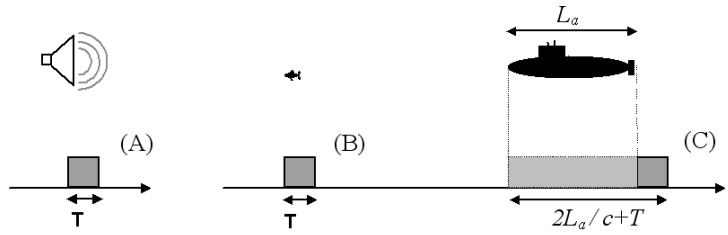

Figure 2.14 Lengthening of a time signal. Signal transmitted (*A*), backscattered by a point target (*B*) and by a long target (*C*).

A similar effect of signal lengthening occurs during reflections and backscattering from the interfaces; the signal transmitted intercepts part of the surface or the seabed, and the signal reflected reproduces the extension of this reflector; hence this concept of geometrical lengthening is a basic tool for understanding the echo formation from the ocean interfaces.

And finally, as we saw earlier, the global time structure of the signal received depends on the multipaths.

In all cases, the modeling of underwater acoustic signals must be complemented with the fluctuating and random characteristics of the propagation medium. This leads one to consider statistically the physical processes, and construct models accordingly. These processes are discussed in the second part of Chapter 4.

2.6 SOUND VELOCITY IN THE OCEAN

2.6.1. Velocity parameters

Sound velocity depends on both temperature, salinity and hydrostatic pressure (and hence depth).

- *Temperature*. Globally, sea water temperature decreases from the surface to the seabed; but there are many variations from this general trend. The time and space variability is maximal in the shallower layers (due to surface mixing, solar heating, currents, external inputs), but decreases with depth. Beyond a typical depth (usually around 1000 m in open oceans, but shallower in closed seas: e.g., 100–200 m in the Mediterranean), the average temperature remains stable, decreasing very slowly with depth and varying very little from one place to the other. A fine temperature microstructure gets added to the average temperature profile, and causes local random acoustic fluctuations.
- *Depth*. Hydrostatic pressure[11] makes the sound velocity increase with depth, because of variations in the compressibility coefficient. This increase is linear as a first approximation, of around 0.017 m/s per meter down.
- *Salinity*. Sea water is made of a mix of pure water and dissolved salts (NaCl, $MGSO_4$, ...). The salt mass percentage defines salinity, expressed in *practical salinity units*[12] or p.s.u. Salinity in the large ocean basins (Atlantic, Pacific and Indian Oceans) is on average about 35 p.s.u., but locally it can vary strongly as a

[11] Hydrostatic pressure in sea water is given with a good accuracy by Leroy's formula (Leroy, 1968): $P = [1.0052405(1 + 5.28 \times 10^{-3} \sin^2 \phi)z + 2.36 \times 10^{-6} z^2 + 10.196] \times 10^4$, in which the pressure P is in Pa, ϕ is the latitude (in °), and z is the depth (in meters). A more complete model may be found in (Leroy and Parthiot, 1998).

[12] Salinity was traditionally expressed as per-thousand of the mass, noted as ‰ or p.p.t. (part per thousand); it is now expressed in *practical salinity units*. The numerical values do not change from one system to the other.

function of the hydrological conditions. In closed seas, the average value of the salinity can be quite different from 35 p.s.u., depending on whether evaporation is more important (e.g., 38.5 p.s.u. in the Mediterranean), or fresh water input is more important (e.g., 14 p.s.u. in the Baltic). At a given location, salinity usually varies only slightly with depth (1 to 2 p.s.u.), excepting possibly in the shallowest layers (where there might be stronger variations in local freshwater input configurations: river estuaries, ice melt, etc.) or even exceptionally in deeper layers (the so-called *meddies*, or Mediterranean-water lenses drifting at depths around 1,500 m in the North-East Atlantic).

2.6.2 Sound velocity models

The impact of sound velocity variations on acoustic propagation was first noticed and has been systematically studied from the 1940s (NDRC, 1946). However, local velocity measurements are quite difficult to perform accurately, whereas its constitutive parameters (temperature, salinity, depth) are much more easily quantified. Parametric models have been extensively studied, and several sound velocity models are now available in the literature (e.g., Wilson, 1960; Leroy, 1969; DelGrosso, 1974; Medwin, 1975; Chen and Millero, 1977). They all refer to a common corpus of experimental data obtained under controlled laboratory conditions and enriched along the years, to which they try to fit as closely as possible.

As a first approximation and for simplicity, one can use the formula proposed by Medwin (1975), however limited to a 1,000-m depth:

$$\begin{aligned} c =& 1449.2 + 4.6T - 0.055T^2 + 0.00029T^3 \\ &+ (1.34 - 0.01T)(S - 35) + 0.016z \end{aligned} \tag{2.52}$$

where c is the sound velocity, in m/s; T is the temperature, in °C; z is the depth, in m; S is the salinity, in p.s.u.

More recent and accurate models are, however, recommended. One such model, proposed by Chen and Millero (1977), is now widely used. It is endorsed by UNESCO, and used as a standardized reference model:

$$c = c_0 + c_1 P + c_2 P^2 + c_3 P^3 + AS + BS^{3/2} + CS^2 \tag{2.53}$$

The first four terms correspond to the contribution of pure water, and the next three terms to salinity, all being influenced by pressure (or depth). c is the sound velocity, in m/s; P is the hydrostatic pressure, in bars ($P = 0$ at the surface, although the actual pressure there equals about 1 bar); T is the temperature in °C; and S is the salinity in p.s.u.

The parameters of the model are:

$$
\begin{cases}
c_0 = 1402.388 + 5.03711T - 5.80852 \times 10^{-2}T^2 + 3.3420 \times 10^{-4}T^3 \\
\qquad -1.47800 \times 10^{-6}T^4 + 3.1464 \times 10^{-9}T^5 \\
c_1 = 0.153563 + 6.8982 \times 10^{-4}T - 8.1788 \times 10^{-6}T^2 + 1.3621 \times 10^{-7}T^3 \\
\qquad -6.1185 \times 10^{-10}T^4 \\
c_2 = 3.1260 \times 10^{-5} - 1.7107 \times 10^{-6}T + 2.5974 \times 10^{-8}T^2 - 2.5335 \times 10^{-10}T^3 \\
\qquad +1.0405 \times 10^{-12}T^4 \\
c_3 = -9.7729 \times 10^{-9} - 3.8504 \times 10^{-10}T - 2.3643 \times 10^{-12}T^2 \\
A = A_0 + A_1P + A_2P^2 + A_3P^3 \\
A_0 = 1.389 - 1.262 \times 10^{-2}T + 7.164 \times 10^{-5}T^2 + 2.006 \times 10^{-6}T^3 - 3.21 \times 10^{-8}T^4 \\
A_1 = 9.4742 \times 10^{-5} - 1.2580 \times 10^{-5}T - 6.4885 \times 10^{-8}T^2 + 1.0507 \times 10^{-8}T^3 \\
\qquad -2.0122 \times^{-10} T^4 \\
A_2 = -3.9064 \times 10^{-7} + 9.1041 \times 10^{-9}T - 1.6002 \times 10^{-10}T^2 + 7.988 \times 10^{-12}T^3 \\
A_3 = 1.100 \times 10^{-10} + 6.649 \times 10^{-12}T - 3.389 \times 10^{-13}T^2 \\
B = -1.922 \times 10^{-2} - 4.42 \times 10^{-5}T + (7.3637 \times 10^{-3} + 1.7945 \times 10^{-7}T)P \\
C = -7.9836 \times 10^{-6}P + 1.727 \times 10^{-3}
\end{cases}
\tag{2.53a}
$$

Although widely used, the model of Chen and Millero presents some defects: its behavior with depth is not accurate enough (Millero and Li, 1994), and it is expressed as a function of pressure, while most often a dependence with depth is preferred by users. This led Leroy to propose a simplified equation (Leroy *et al.*, 2008), both simplifying the numerical expressions, and ensuring an excellent agreement with the reference experimental results:

$$
\begin{aligned}
c = {} & 1402.5 + 5T - 5.44 \times 10^{-2}T^2 + 2.1 \times 10^{-4}T^3 + 1.33S - 1.23 \times 10^{-2}ST \\
& + 8.7 \times 10^{-5}ST^2 + 1.56 \times 10^{-2}Z + 2.55 \times 10^{-7}Z^2 - 7.3 \times 10^{-12}Z^3 \\
& + 1.2 \times 10^{-6}Z(\phi - 45) - 9.5 \times 10^{-13}TZ^3 + 3 \times 10^{-7}T^2Z + 1.43 \times 10^{-5}SZ.
\end{aligned}
\tag{2.54}
$$

where ϕ is the latitude in degrees.

Seawater contains many *heterogeneities*: bubble layers close to the surface, living organisms (e.g., fish, plankton), mineral particles in suspension, etc. These are as many potential scatterers of acoustic waves, especially at high frequencies, and cause perturbations of the acoustic characteristics (sound velocity and absorption).

Bubble clouds are a dual-phase medium, in which sound velocity can be significantly different from the sound velocity in sea water, particularly if the resonant frequency of a portion of the bubble population is close to the frequency of the acoustic wave. The velocity c_{bw} in water filled with gas bubbles of identical radius a is related to the sound velocity c_w in normal sea water:

$$c_{bw} = c_w \left[1 - \frac{aNc_w^2}{2\pi f^2} \frac{f_0^2/f^2 - 1}{(f_0^2/f^2 - 1)^2 + \delta^2} \right] \tag{2.55}$$

where N is the number of bubbles per unit volume, f_0 is their resonant frequency, and δ is the attenuation constant (see Section 3.3.3).

2.6.3 Sound velocity measurements

Several types of devices may be used for *in situ* measurement of sound velocity. A *velocimeter* directly measures the sound velocity (either from time-of-flight or from phase shift) for a high-frequency wave transmitted over an accurately calibrated distance. This instrument is very delicate, since it must be insensitive to constraints caused by important variations in temperature and hydrostatic pressure. It can typically provide an accuracy of a few tens of cm/s.

When very accurate hydrology measurements are needed, the dedicated tool is the *CTD probe*, dipping along a stopped ship and using a dedicated cable and winch. This device provides very fine measurements of temperature, salinity and depth (and can perform water sampling too) which can then be converted into sound speed values. Such reference measurements, very classical in physical oceanography cruises, are unfortunately quite time-consuming, and hence are used, in an underwater acoustics context, as a benchmark in case of doubts about the results obtained with rougher measurements rather than as a routine operation.

In this respect, the most common and simple device is the bathythermograph, often known as *XBT* (*eXpendable BathyThermograph*) probe. This sensor only measures water temperature as a function of depth. Obtaining the sound velocity profile (SVP) implies accessing independently the salinity profile; this can be done either by a conductance meter, integrated inside the same device (which is then an *XCTD* probe, more expensive and less widespread); or more often by using hydrology databases (e.g., Levitus, 1982), giving the average values of salinity to a sufficient accuracy. The bathythermograph is by far the most popular instrument for operational sound speed profile measurements in an underwater acoustic context; the most widespread models[13] can be launched from a ship in motion (instead of strictly measuring *depth* they provide a *time-dependent* temperature, converted to depth thanks to an accurate control of their descent speed based on the probe shape).

Although XBT and XCTD probes often provide a well-adapted solution for many operational needs, they remain *local measurement* devices. For some specially

[13] From the Sippican company (USA), who gained a worldwide exclusivity with this product.

demanding configurations, they may be replaced by sensors towed at continuously-varying depth, providing high-density sampling of hydrological characteristics along the ship's route.

The accurate knowledge of sound velocity profiles over a particular area is necessary for many sonar applications. For example, in ASW, an overall knowledge of the sound velocity field is necessary to optimize detection capabilities and strategies. In bathymetry surveys, the sounding quality depends on an extremely accurate compensation of the sound ray trajectories.

Note that many ships are equipped with hull-mounted *thermometers* or *thermosalinometers*, or even *velocimeters*, able to provide information needed for computing the sound-speed value at the sonar arrays. These data, continuously recorded, come in complement of the SVP measured otherwise.

2.6.4 Depth-velocity profiles

For sonar purposes, the hydrological environment can often be approximated as *horizontally stratified*; sound velocity is then assumed to depend strictly on depth, which greatly simplifies propagation modelling and interpretation. The resulting sound velocity profiles (SVP) are made up of several characteristic parts (Figure 2.15):

- A homogeneous layer (*mixed layer*), of constant sound velocity, is often present in the first few meters. It corresponds to the mixing of superficial water through surface agitation.
- A *surface channel* corresponds to sound velocity increasing from the surface down. This channel is often due to a shallow isothermal layer appearing in

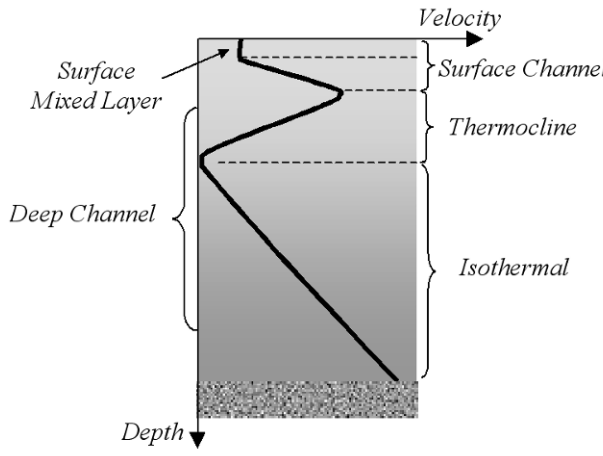

Figure 2.15 The different elements of a typical sound-velocity profile. Sound velocity is represented on the x-axis, depth on the y-axis (going down).

winter conditions, but can also be caused by water that is very cold in surface (e.g. ice melting), or by an input of fresh water near river estuaries.

- A *thermocline* is a monotonous variation of temperature with depth. It is most often negative (temperature decreasing usually from the surface to the bottom), and then induces a velocity decrease with depth. It can be seasonal (close to the surface) or permanent.
- A *deep channel* corresponds to a sound velocity minimum (e.g., between a negative thermocline and a deep isothermal layer). The average depth-velocity profile of large ocean basins shows a deep channel between a few hundred meters and 2,000 meters.
- An *isothermal layer* is at a constant temperature. Hence sound velocity increases linearly with depth, because of the hydrostatic pressure. The ocean deeper layers are approximately isothermal. So are the sound velocity profiles in closed seas (e.g., the Mediterranean), or in shallow waters under winter conditions.

These different components can combine to form very varied SVP shapes, depending on environment conditions. Local processes can complicate matters:

- At intermediate spatial scales (*mesoscale*, tens of kilometers), the average velocity profiles are modified by the presence of currents, thermal fronts and eddies. These processes strongly perturb propagation; conversely, they can be studied by acoustic means (see *ocean acoustic tomography*, Section 7.4.2).
- At high latitudes, the presence at the surface of very cold water coming from the melting of the ice pack causes a very noticeable minimum velocity.

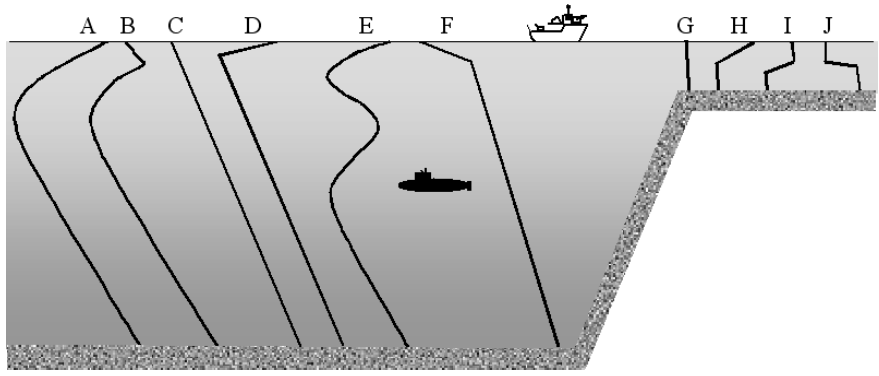

Figure 2.16 Generic sound-velocity profiles. Sound velocity is represented on the x-axis, depth on the y-axis (going down). From left to right: (A) summer SOFAR[14] channel; (B) winter SOFAR; (C) winter Mediterranean (isothermal); (D) summer Mediterranean; (E) NE Atlantic (with Mediterranean water intrusion); (F) polar; (G) winter shallow water; (H) summer shallow water; (I) autumn shallow water; (J) shallow water with fresh water at the surface.

[14] SOFAR: SOund Fixing And Ranging (see Section 2.7.3 for details).

- As an example of water mass exchange between ocean basins, in the Gibraltar Strait, Mediterranean waters intrude into the North-East Atlantic, causing there a warmer and more salty layer, with a marked local maximum of velocity between 1,000 and 2,000 m in depth.
- Near river estuaries, fresh water input creates a slower shallow layer, inducing important perturbations (the velocity difference between fresh water and sea water at given depth and temperature is ca. 40 m/s).

Other factors are the *internal waves* and *internal tides*, related to variations in water density with depth. When propagating, they create fluctuations of sound velocity profiles over large spatial scales. Their effect on acoustic propagation has been studied since the 1970s (see, e.g. Flatté 1979, for a detailed study).

Some generic depth-velocity profiles are shown in Figure 2.16 for different types of water column. They illustrate the rich variety of possible configurations, corresponding to varied propagation phenomena and resulting sound field structures; basic elements about this topic are given in Section 2.8.

2.7 GEOMETRICAL INVESTIGATION OF THE ACOUSTIC FIELD

N.B. In underwater acoustic modeling, it may be more convenient to deal with either grazing angles (referenced relatively to the horizontal) or incidence angles (referenced relatively to the vertical). Logically enough, the first convention is preferred in applications related to in-water "horizontal" propagation geometries involving multipaths (mainly military sonar applications, but also ocean acoustic tomography). And the second convention is chosen for vertical and oblique transmission applications (e.g., echosounders and imaging sonars). In the following, we shall use both conventions, with the notation below to avoid confusion:

- *horizontal grazing angles* will be noted β; they will mainly be used in this chapter, devoted to propagation processes;
- *vertical incident angles* will be noted θ; they will be used also in Chapter 3 (refraction and backscattering) and in Chapter 8 (about seafloor mapping sonars).

2.7.1 Depth-velocity profile refraction

Let us now look at the modifications of the characteristics of a plane wave, at the interface between two homogeneous fluids with different sound velocities (c_1, c_2) (Figure 2.17). The change of sound velocity between the two media induces specular reflection of the wave in the first medium (along a direction symmetrical to the normal at the incidence point), and refraction of the wave in the second medium, at an angle given by the famous Snell-Descartes law (see Appendix A.3.1):

$$\frac{\cos \beta_1}{c_1} = \frac{cos\, \beta_2}{c_2} \tag{2.56}$$

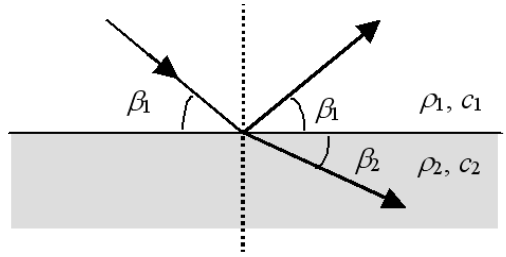

Figure 2.17 Reflection and refraction of a plane wave, due to the change in sound velocity at the interface ($c_2 > c_1$).

Equation (2.56) can only be written if $\cos\beta_2 \leq 1$ (i.e. for $\cos\beta_1 \leq c_1/c_2$). The limit angle given by the equation

$$\beta_c = \arccos(c_1/c_2) \tag{2.57}$$

is the *critical angle* for the interface. For angles β smaller than β_c (low-grazing incidence), there is *total reflection*; transmission into the second medium is then impossible.

The Snell-Descartes law can be applied to a series of constant-velocity layers, located by the indices $i = 1, 2, \ldots, N$. The law then becomes:

$$\frac{\cos\beta_1}{c_1} = \cdots = \frac{\cos\beta_i}{c_i} = \frac{\cos\beta_{i+1}}{c_{i+1}} = \cdots = \frac{\cos\beta_N}{c_N} \tag{2.58}$$

It can be used to describe the behavior of a wave propagating in a medium with non-constant velocity, varying with a coordinate z. By taking the limit case of infinitely thin layers, the refraction relation comes into the general expression:

$$\frac{\cos\beta(z)}{c(z)} = \text{constant} \tag{2.59}$$

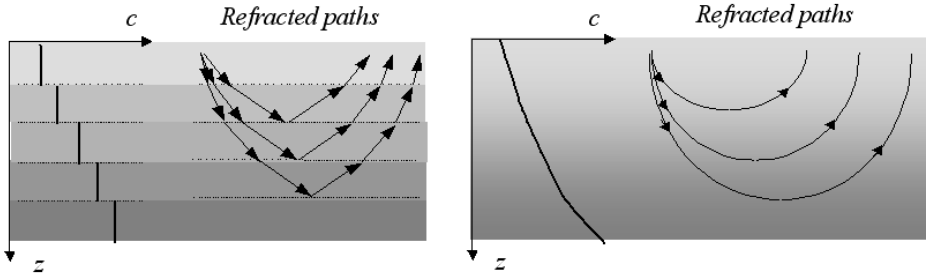

Figure 2.18 Refraction of a wave with a discontinuous (left) and continuous (right) variation of the sound velocity with depth.

Continuous changes in the sound velocity of a propagation medium will progressively change the wave initial direction (Figure 2.18); the wave vector orientation depends on the local velocity. If the velocity gradient is vertical (which is most common), an increase in velocity will decrease the grazing angle and refract the wave path toward the horizontal. If the velocity increases enough, an acoustic path inclined relative to the horizontal can undergo *total refraction*. Conversely, a decrease in velocity will increase the grazing angle of the wave. The geometrical path followed by a wave between two points is called an *acoustic ray*.

2.7.1.1 Case of a linear sound speed profile

If the depth-velocity law is linear in $c(z) = c_0 + g(z - z_0)$, where g is the velocity gradient, the Snell-Descartes relation becomes:

$$\cos\beta(z) = \frac{c(z)}{c_0}\cos\beta_0 = \left(1 + \frac{g}{c_0}(z - z_0)\right)\cos\beta_0 \tag{2.60}$$

This is depicted in Figure 2.19.

For any circle in the (x, y) plane (Figure 2.19), the general relations between the Cartesian co-ordinates of a point, the slope angle β (defined by the tangent to the circle) and the circle radius R_c may be written as:

$$z - z_0 = R_c(\cos\beta - \cos\beta_0) \tag{2.61}$$

where (x_0, z_0) and β_0 define a reference point along the circle. The cosine of the angle at a given point can then be related to z by:

$$\cos\beta(z) = \cos\beta_0 + \frac{z - z_0}{R_c} \tag{2.62}$$

Formally, this is similar to equation (2.60). An important result is therefore that, in the case of a linear sound speed profile of gradient g, the waves are refracted along circles of radii R_c given by the input angle value β_0 at depth of velocity c_0:

$$R_c = \frac{c_0}{g\cos\beta_0}. \tag{2.63}$$

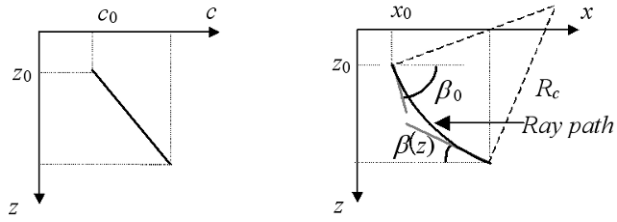

Figure 2.19 Geometry and notation of a circular ray in a linear velocity gradient.

2.7.1.2 Generalization

Geometric acoustics[15] (the theory of which is exposed in Appendix A.2.7) aims at modeling the structure of the acoustic field as a set of paths (or *acoustical rays*) following the basic principles:

- refraction of the propagation direction by sound speed changes, according to the Snell-Descartes law;
- specular reflection at the interfaces;
- intensity losses along rays, through *geometric divergence* (i.e., spherical divergence being then modified by refraction), through absorption along the paths, and through reflections on the interfaces;
- resulting field at a receiver modeled by summing the contributions of the various rays, with appropriate amplitudes and delays.

It is therefore a generalization of the basic model of image sources presented in Section 2.4.3, because it accounts for refraction by the sound velocity profile.

We saw that, for a linear profile, a very simple form of refracted paths (arcs of circles) is obtained. Other analytical solutions can be derived for canonical velocity profiles other than the linear case; but they are of little actual interest for practical applications.

In practice, the generalization to more complicated sound speed configurations (Figure 2.16) can be done by approximating the sound speed profile by elementary layers with constant gradients. This allows tracing the paths for any velocity condition using elementary circular ray paths. Moreover, beyond the simple tracing of acoustic paths and its attractive intuitive pictorial display, this *ray method* can provide the *transmitted acoustic intensity* (the spreading loss being estimated by calculating the spacing between two neighboring rays), and *travel times* (from integration along the paths). The main formulas of this approach are provided in the next section. An alternate method consists in numerically integrating the eikonal equation using a finite-differences scheme. This allows to account for arbitrary (non-stratified) velocity profiles (see Section 2.7.4).

2.7.2 Sound ray calculations in a stratified ocean

Let $c(z)$ be the sound velocity profile. The profile is approximated by a finite number $N+1$ of points (indices $n = 0, \ldots, N$) defining N layers (indices $n = 1, \ldots, N$); inside each layer the velocity is assumed to vary linearly (Figure 2.20).

[15] The theoretical bases of geometric acoustics are formally and rigorously derived from the wave equation. It can be shown that, as long as the frequency is high enough that the sound speed variation over one wavelength remains small, the Helmholtz equation leads to an approximation named "eikonal equation", linking the components of the plane wave-like vector to the local velocity conditions. This approach is summarized in this book as Appendix A.2.2.

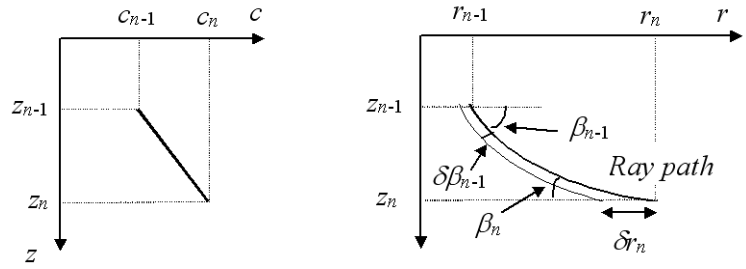

Figure 2.20 Geometry and notation of a ray in a particular layer n.

In layer n, the sound velocity gradient reads:

$$g_n = \frac{c_n - c_{n-1}}{z_n - z_{n-1}} \tag{2.64}$$

The Snell-Descartes law reads:

$$\frac{\cos\beta_n}{c_n} = \frac{\cos\beta_{n-1}}{c_{n-1}} = \text{constant} \tag{2.65}$$

A ray with an entry angle β_{n-1} in the layer will undergo circular refraction with the curvature radius:

$$R_{cn} = \frac{c_{n-1}}{g_n \cos\beta_{n-1}} \tag{2.66}$$

The location (r, z) of the current point[16] in the layer is given by:

$$\begin{cases} r - r_{n-1} = \dfrac{c_{n-1}}{g_n \cos\beta_{n-1}} (\sin\beta_{n-1} - \sin\beta) \\ z - z_{n-1} = \dfrac{c_{n-1}}{g_n \cos\beta_{n-1}} (\cos\beta - \cos\beta_{n-1}) \end{cases} \tag{2.67}$$

where β is the local angle, positive or negative depending on whether the ray is going respectively down or up relative to the horizontal (Figure 2.21).

The travel time in layer n is obtained by integration of the elementary delays along the path (see Appendix A.2.2.1):

$$t_n = \int_{z_{n-1}}^{z} \frac{dz}{c(z)\sin\beta(z)} = \frac{1}{g_n} \ln\left(\tan\left(\frac{\beta_{n-1}}{2} + \frac{\pi}{4}\right) \Big/ \tan\left(\frac{\beta}{2} + \frac{\pi}{4}\right) \right) \tag{2.68}$$

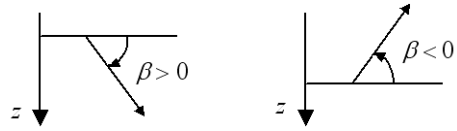

Figure 2.21 Sign convention for the ray angles.

[16] The horizontal coordinate is now taken to be the axial radius r instead of the Cartesian x used in Section 2.7.1.1. This underlines the cylindrical symmetry of the configuration around vertical axis z.

Using the relation:

$$\tan\left(\frac{\beta}{2}+\frac{\pi}{4}\right)=\frac{1+\sin\beta}{\cos\beta} \tag{2.69}$$

one can therefore derive the equivalent expressions for the travel time:

$$t_n=\frac{1}{g_n}\ln\left(\frac{\cos\beta}{\cos\beta_{n-1}}\,\frac{1+\sin\beta_{n-1}}{1+\sin\beta}\right)=\frac{1}{g_n}\ln\left(\frac{c}{c_{n-1}}\,\frac{1+\sin\beta_{n-1}}{1+\sin\beta}\right) \tag{2.70}$$

The curvilinear path length is:

$$s_n=\int_{z_{n-1}}^{z}\frac{dz}{\sin\beta(z)}=\frac{c_{n-1}}{g_n\cos\beta_{n-1}}\,(\beta_{n-1}-\beta) \tag{2.71}$$

This quantity is used to calculate the propagation loss by absorption.

When reaching an interface (sea surface or bottom) with angle β_s, the ray is reflected specularly, with an angle $\beta_s'=-\beta_s$. It then follows a reflected path symmetrical to its incident path, relative to the impact point defined by $r=r_s$.

Across a gradient change, r, z and β must be continuous at the transition; the same follows for $\partial r/\partial\beta_0$, for geometric spreading (see below for more details). These conditions being fulfilled, all the above formulas are applicable layer after layer.

2.7.3 Losses from geometric spreading

Computing the losses from geometric spreading mainly consists in following the evolution of a geometric beam section with an infinitesimal aperture $\delta\beta_0$ at the source. The intensity loss[17] at the point of range r relative the intensity at the point of range r_0 in a homogeneous medium reads:

$$\frac{I(r)}{I(r_0)}=\frac{dS(r_0)}{dS(r)}=\frac{\cos\beta_0}{r\left|\dfrac{\partial r}{\partial\beta_0}\sin\beta\right|} \tag{2.72}$$

or, expressing this transmission loss in dB:

$$TL=10\log\left[\left|\frac{\partial r}{\partial\beta_0}\sin\beta\right|\frac{r}{\cos\beta_0}\right] \tag{2.73}$$

[17] The loss is sometimes expressed as a convergence factor η (*focusing factor*, or *propagation anomaly*, depending on the authors). This factor corresponds to the ratio of the propagation loss to its value at the same point in a homogeneous medium:

$$\eta=\frac{r\cos\beta_0}{\left|\dfrac{\partial r}{\partial\beta_0}\sin\beta\right|}$$

This is a multiplicative correction to apply to the spherical loss factor in $1/r^2$. Values of η larger or smaller than unity show zones with intensities larger or smaller than the field of a spherical wave.

The difficulty of this expression lies in the term $|\partial r/\partial\beta_0|$, whose evolution must be followed layer after layer, with the formulas respectively giving the evolution of the beam aperture (Equation 2.74) and the evolution of the beam section projected along r (Equation 2.75):

$$\delta\beta_n = \frac{\tan\beta_{n-1}}{\tan\beta_n}\,\delta\beta_{n-1} \tag{2.74}$$

$$\begin{aligned}\delta r_n &= \delta r_{n-1} - (r_n - r_{n-1})\,\frac{\delta\beta_{n-1}}{\cos\beta_{n-1}\sin\beta_n} \\ &= \delta r_{n-1} - (r_n - r_{n-1})\,\frac{\tan\beta_0}{\sin\beta_{n-1}\sin\beta_n}\,\delta\beta_0\end{aligned} \tag{2.75}$$

The above expression of the loss is not valid when $\sin\beta \to 0$. This is only because we chose to project the ray section on the r axis. It would be enough to replace $\left|\dfrac{\partial r}{\partial\beta_0}\sin\beta\right|$ with $\left|\dfrac{\partial z}{\partial\beta_0}\right|\cos\beta$.

The geometric approach to transmission losses is no longer valid when $|\partial r/\partial\beta_0| \to 0$; the convergence of a geometric beam would create locally infinite intensities. In such areas of the sound field, called *caustics*, we are at the limits of the geometric method validity. Ideally, one should then compute the exact solution of the propagation equation (e.g., Brekhovskikh and Lysanov, 1992), and apply locally the field thus computed.

2.7.4 Application of geometric acoustics

We have just seen that it is possible to build acoustic paths for rather complex velocity variations, just by using elementary geometric constructs, which can be easily implemented numerically on computers. We restricted ourselves to a variation of velocity with depth only, but it is perfectly possible to trace rays with velocities varying as a function of two or three spatial coordinates. The best approach is then not to look for analytical forms (like the arc of circle in Section 2.7.1), but to solve directly and numerically the eikonal equation, following the ray path with a small numerical increment (the *Runge-Kutta finite-difference* technique is often used for this application).

Ordinarily, ray tracing software calculate all the ray paths emitted in an angular sector (in the vertical plane) close to the source, with a relatively small increment (typically a tenth of a degree or less), up to the maximum range of interest. This first computation step having been achieved, to ascertain the rays arriving at a particular reception point, one must determine the couples of rays emitted consecutively whose paths border the target point on both sides. Each couple thus determined corresponds to a given "history" of the ray (number of reflections and refractions). The exact characteristics of the rays arriving at the receiver (angle, time, phase, transmission loss) are finally computed by interpolating between the characteristics of the two rays of each selected couple.

The geometric description of the acoustic field is used in most applications aiming at the accurate determination of propagation times and angles: bathymetry measurements by sounders, acoustic ocean tomography, etc. This technique has many advantages, which explains its predominance. First, its graphical representation of the acoustic field structure as paths is easily and intuitively understandable. Second, it describes accurately the sound field structure at a receiving point with propagation times and directions of arrival (which are key parameters for many applications) by numerical calculations that are relatively simple and rapid. Finally, although approximate, its prediction of intensity levels is good enough in most cases. It is clearly inadequate only for very low frequencies (tens or hundreds of Hz, depending on the water depth), for which wave processes dominate the purely geometric aspect of refractions.

2.8 UNDERWATER ACOUSTIC PROPAGATION: CASE STUDIES

We investigate here a few typical propagation configurations determined by the depth-velocity profile. These cases are illustrated with acoustic ray tracing, and considerations about the time-domain response and transmission loss.

2.8.1 Constant-velocity profile

In configurations with a constant sound speed c, the acoustic rays are rectilinear, and the tracing of the acoustic field is very easily obtained (Figure 2.22), as straight lines bouncing between the surface and the seabed. It is not even necessary to trace rays *stricto sensu*, and in this case the field can be practically described as a sum of contributions from image sources (cf. Section 2.4.3), corresponding to reflections at the interfaces. These contributions are obtained by successive symmetries of the actual source relative to the surface and the bottom.

Each image source corresponds to a particular ray, of easily computable characteristics. The source and receiver being a horizontal distance D away, for a path defined by its source angle β determined in Section 2.4.3, the propagation time is given by the oblique range $R(\beta) = \dfrac{D}{\cos\beta}$:

$$t(\beta) = \frac{R(\beta)}{c} = \frac{D}{c\cos\beta} \tag{2.76}$$

The equivalent horizontal velocity of the path is:

$$V(\beta) = c\cos\beta \tag{2.77}$$

The propagation loss is given by the oblique distance travelled $R(\beta)$:

$$TL(\beta) = 20\log R(\beta) + \alpha R(\beta)$$

so, like R, it increases with β (i.e., the more tilted the ray path, the greater the loss).

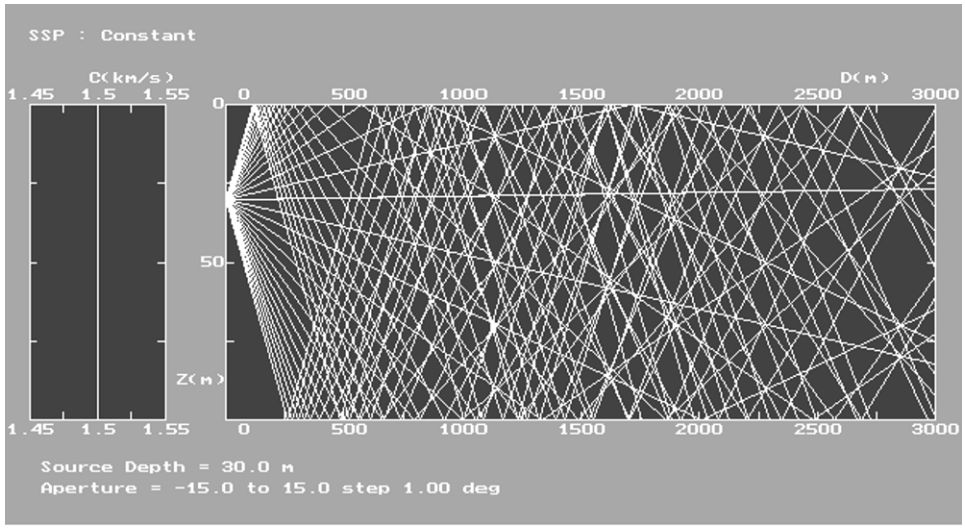

Figure 2.22 Ray tracing for a constant-velocity configuration.

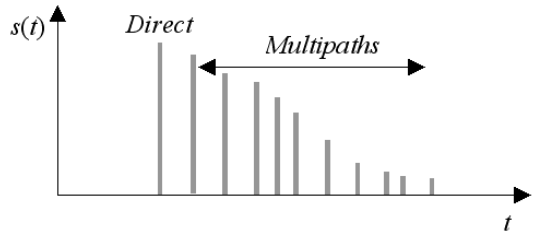

Figure 2.23 Impulse response for an constant-velocity channel: the direct path arrives first, the amplitude of multipaths decrease with their order (longer oblique length, more reflections).

Reflection losses increase too as the grazing angle increases (see Chapter 3 for more details). The direct path, corresponding to the minimal value of β and R, arrives first and has the maximum amplitude; the multiple reflected paths follow it with decreasing amplitudes (Figure 2.23) due both to longer path lengths and to higher interface reflection losses (see also Figure 2.7).

Although clearly too idealized, the approximation of a constant-velocity profile is very useful in many contexts. It is a good approximation for many configurations of shallow-water propagation in winter-like isothermal conditions (the velocity increase due to pressure effect may be neglected over depths a few tens of meters), or even in deeper water at sufficiently short ranges (when the ray-bending effect of steep ray paths is of secondary importance). Also it is used by default in the evaluation of sonar system performance. Finally, it is often used as a reference configuration, and is very useful for teaching purposes.

2.8.2 Isothermal profile

When the temperature does not vary with depth, the sound velocity linearly increases with depth because of the hydrostatic pressure effect, with a gradient around 0.017 m/s/m. All the acoustic ray paths are therefore refracted upward, and propagate by successive bounces on the surface (Figure 2.24). This configuration is called a *surface channel*. This hydrological condition is rather common in shallow water; however, as explained above, the resultant acoustic field is then close to the constant-velocity case, the small velocity change across a shallow water depth causing only very slight refraction effects. More significantly, isothermal profiles are also found in deep water: they can then correspond either to a layer close to the surface, or even to the entire water column[18], and the refraction effects are then fully developed.

The isothermal configuration is described by the linear law $c(z) = c_s + gz$ as a function of depth z, with $c_s = c(0)$. The rays are then arcs of circles, reflected by the surface (Figure 2.24). They show a periodic structure, with a *horizontal cyclical distance* $D_C(\beta_s)$ for a ray striking the surface with angle β_S; from (2.67):

$$D_C(\beta_S) = 2\,\frac{c_S}{g}\tan\beta_S \tag{2.78}$$

The maximal possible angle (for the field to stay trapped inside the surface channel) corresponds to a ray whose turning point with respect to z axis is just at the lower depth ($z = H$) of the channel (Figure 2.24); hence its value at the surface is given by the ratio of velocities at each end of the profile:

$$\cos\beta_{S0} = \frac{c_S}{c(H)} \quad \text{i.e. roughly} \quad \beta_{S0} \approx \sqrt{\frac{2gH}{c_S}} \tag{2.79}$$

Such an insonification process of the medium is finally rather homogeneous on the average (Figure 2.25), but it favors upper layers if the acoustic source is shallow, since the concentration of rays with short cycle length is higher close to the surface.

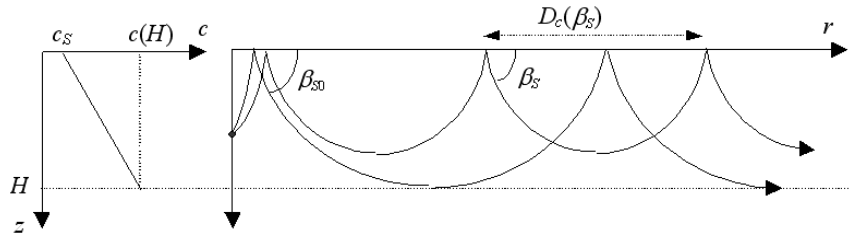

Figure 2.24 Ray geometry for an isothermal sound velocity profile.

[18] This is, for example, the case in the Mediterranean Sea, with a remarkably stable winter temperature around 13°C over the water depth; or at high latitudes in polar waters, where the velocity profiles, although not strictly isothermal, increase monotonously from the surface down to the bottom, and create the same type of propagation.

Using formula (2.68), the propagation time over one cycle reads:

$$T_C(\beta_S) = \frac{2}{g}\ln\left(\tan\left(\frac{\beta_S}{2}+\frac{\pi}{4}\right)\right) \approx \frac{2}{g}\left(\beta_S + \frac{\beta_S^3}{6}\right) \tag{2.80}$$

where the approximation holds for small grazing angle values. And the corresponding mean horizontal velocity is:

$$V(\theta_S) = \frac{D_C}{T_C} \approx c_S\left(1+\frac{\beta_S^2}{6}\right) \tag{2.81}$$

One can therefore see that the fastest paths correspond to the highest β_S (i.e. the largest arcs of circle, see Figure 2.25). This contradicts physical intuition (based on the constant-velocity case) that the "horizontal" paths, being shorter, should arrive first. This apparent paradox can be explained by considering that these high-β_S rays have indeed followed the longest curvilinear distance, but in regions with higher velocities: the increase in propagation velocity overcompensates the increase in distance.

Using the equations of Section 2.7.3, the intensity loss by geometric spreading between two points at a horizontal distance r from each other can be written as:

$$\begin{aligned} TL &= 10\log\left(\left|r\,\frac{c_0\sin\beta_0\sin\beta}{g\cos^3\beta_0}\left(\frac{2n}{\sin\beta_S}-\frac{1}{\sin\beta_0}+\frac{1}{\sin\beta}\right)\right|\right) \\ &\approx 10\log\left(\frac{r^2|\sin\beta_0\sin\beta|}{\cos^2\beta_0\sin^2\beta_S}\right) \end{aligned} \tag{2.82}$$

the final approximation holding for a sufficiently high number $n = r/D_C(\beta_S) = rg/(2c_S|\tan\beta_S|)$ of surface reflections.

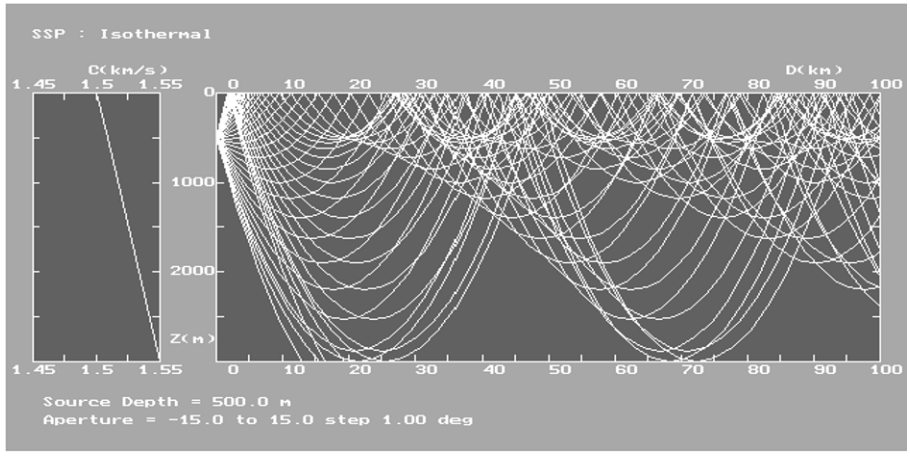

Figure 2.25 Ray tracing for an isothermal sound speed profile.

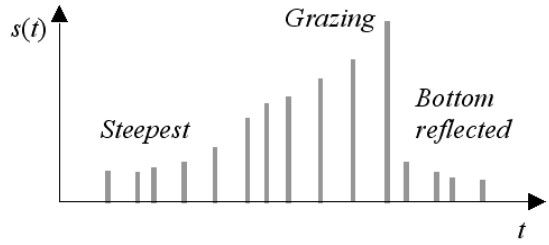

Figure 2.26 Impulse response for an isothermal channel: the steepest rays arrive first with the smallest amplitudes (longer paths, higher surface reflection losses), and the grazing angles come last, with a maximum amplitude; they are followed by the bottom-reflected group.

The impulse response of the medium therefore shows arrivals corresponding first to the highest angles (with maximum value β_{S0}), and last to the most grazing angles (incidentally, with the highest amplitudes) (Figure 2.26). The time spreading of the signal is given by the velocity difference between the slowest (at β_S close to 0) and the fastest (at β_{S0}) rays. Thus it can be approximated as:

$$\Delta t = r\left(\frac{1}{V(0)} - \frac{1}{V(\beta_{S0})}\right) \approx r\,\frac{\beta_{S0}^2}{6c_S} \tag{2.83}$$

Beyond β_{S0}, the rays can strike the bottom and be reflected. Their refracted character is less and less marked as the grazing angle increases, and their general behavior resembles more and more closely the behavior of rectilinear paths in isovelocity conditions, bouncing between the surface and the seafloor: the successive arrivals then correspond to increasing angles, and to decreasing amplitudes.

2.8.3 Deep sound channel

The *deep sound channel* (DSC) is an ocean configuration where the sound velocity decreases from the surface to a minimum value (at a depth z_A named the *channel axis*), and then increases down to the bottom. This case is met in most deep oceanic basins; the temperature usually decreases (*thermocline* layer) from the surface to a deep value of 2°C to 4°C, and below this depth it stays stable, so the SVP is then isothermal. In the following, we will describe the sound velocity profile in the simplified form of two linear segments, of gradients g_1 and g_2 with opposite signs. In the upper part ($z < z_A$), the velocity varies in $c(z) = c_S + g_1 z$, with $g_1 < 0$, decreasing from c_S to c_A. In the deep part ($z > z_A$), it varies in $c(z) = c_A + g_2(z - z_A)$, with $g_2 > 0$, increasing from c_A to c_B next to the seafloor.

2.8.3.1 SOFAR propagation

If the source is close to the channel axis (minimum velocity c_A in z_A), the rays transmitted at grazing angles are trapped between the two gradients since they are

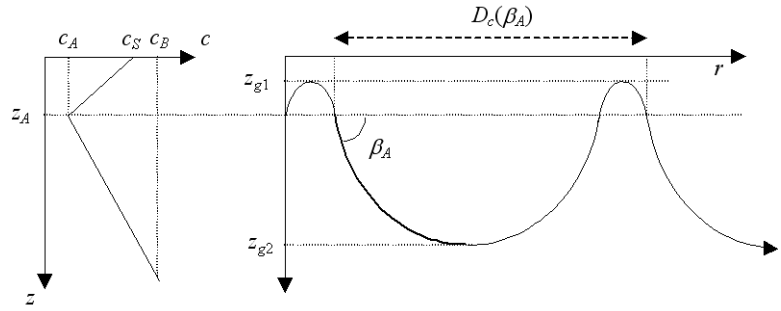

Figure 2.27 Deep-channel ray geometry.

successively refracted upward and downward and can propagate without interacting with the interfaces (Figure 2.27). The condition of existence of this mode of propagation is that the angle β_A of the ray when crossing the axis verifies:

$$\cos\beta_A > \max\left(\frac{c_A}{c_S}, \frac{c_A}{c_B}\right) \tag{2.84}$$

Since most often $c_S < c_B$, this usually reduces to $\cos\beta_A > c_A/c_S$. The cycle length of a ray is then:

$$D_C = 2c_A\left|\tan\beta_A\left(\frac{1}{g_2} - \frac{1}{g_1}\right)\right| \tag{2.85}$$

The depths at the turning points of the ray of angle β_A become:

$$\begin{cases} z_{g1} = z_A + c_A/g_1(1/\cos\beta_A - 1) \\ z_{g2} = z_A + c_A/g_2(1/\cos\beta_A - 1) \end{cases} \tag{2.86}$$

The equations of the isothermal channel can be reused by writing $\dfrac{1}{g_0} = \dfrac{1}{g_2} - \dfrac{1}{g_1}$. For the ray of angle β_A at the axis, the cycle propagation time thus becomes:

$$T_C(\theta_A) = \left|\frac{2}{g_0}\ln\left(\tan\left(\frac{\beta_A}{2} + \frac{\pi}{4}\right)\right)\right| \approx \left|\frac{2}{g_0}\left(\beta_A + \frac{\beta_A^3}{6}\right)\right| \tag{2.87}$$

And the corresponding cycle horizontal distance is:

$$V(\theta_A) = \frac{D_C}{T_C} \approx c_A\left(1 + \frac{\beta_A^2}{6}\right) \tag{2.88}$$

The propagation loss through geometric spreading is approximated, for a sufficiently high number n of cycles, as:

$$TL \approx 10\log\left[\frac{r^2|\sin\beta_0\sin\beta|}{\cos^2\beta_0\sin^2\beta_A}\right] \tag{2.89}$$

In this configuration, the insonification of the medium is quite homogeneous, especially close to the axis (Figure 2.28) because of the large number of rays interfering at any given point of the waveguide. The number of these paths is larger when closer to the channel axis, which corresponds to a configuration that is favorable energetically, and allows very large transmission ranges: because of the absence of energy loss by reflection at the interfaces on the one hand, and because of the concentration of a large number of multiple paths on the other, the loss by geometric spreading is minimal. The absorption of sound in water is then the main limitation. Ranges of several thousands of kilometers can be achieved by using frequencies that are suitably low. This type of propagation is called SOFAR (for *SOund Fixing And Ranging*). It was discovered during Word War II and used for positioning applications at very large ranges. It is now used for acoustic oceanography experiments, transmitting signals to evaluate the variations of sound velocity at the scale of ocean basins (see Section 7.4.2 for more details).

The impulse response of the SOFAR channel is very characteristic (Figure 2.29). It is an extension of the isothermal case: the most tilted rays arrive first, and are distinguishable if the signal's time resolution is high enough. Then the arrivals are increasingly closer in time and higher in intensity. They end with a group arrival of indistinguishable paths corresponding to para-axial propagation. The time spread of the arrivals depends on the distance and the values of velocity at the interfaces and on the axis: typically from 2 s to 10 s at 1,000 km, depending on the depth-velocity profile. Evidently, this makes the transmission of information other than simple detection or measurement of the arrival time of the end peak more complex, unless one uses a large vertical antenna to filter the angles of the arrivals and so decrease their time spreading.

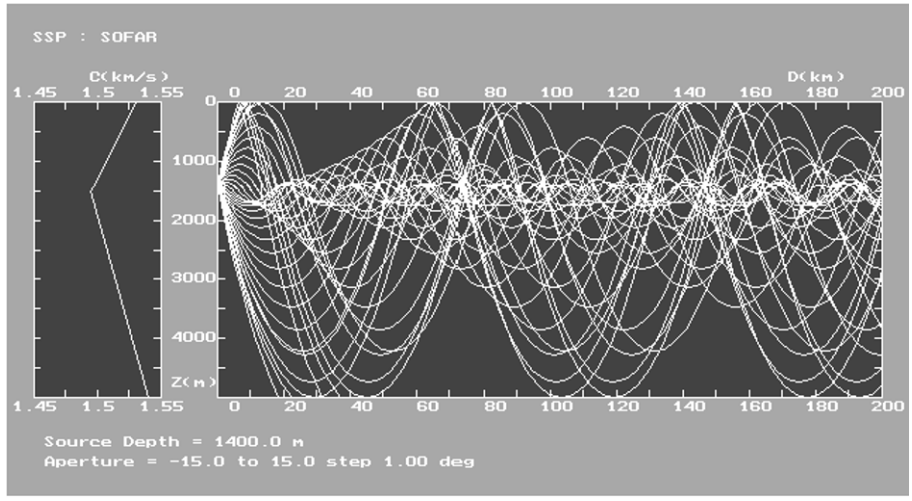

Figure 2.28 SOFAR propagation regime in a deep channel, with a source close to the channel axis.

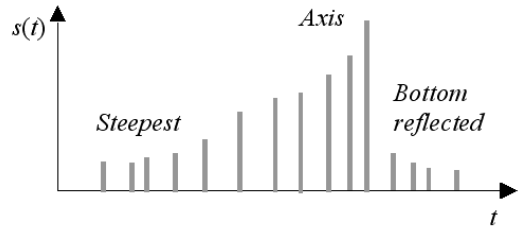

Figure 2.29 Impulse response for a SOFAR channel: the steepest rays arrive first with the smallest amplitudes (longer paths), and the sub-axial rays are last, with a maximum amplitude due to the geometrical divergence; they may be followed by a bottom-reflected group.

2.8.3.2 Shadow and convergence zones

Consider now a source close to the surface. The rays transmitted upwards near the horizontal are rapidly refracted downward, because of the shallow negative gradient (Figure 2.30). The limit ray, tangential to the surface, is emitted upwards at angle β_0:

$$\cos\beta_0 = \frac{c_0}{c_S} \tag{2.90}$$

This ray crosses again the source depth z_0 (Figure 2.30) at the horizontal distance:

$$D_{S0} = \frac{2c_0}{g_1}\tan\beta_0 \tag{2.91}$$

The rays with grazing angles larger than this limit angle will strike the surface, and therefore cross again the source depth at shorter distances.

The ray bundle transmitted in the angular sector $[0, \beta_0]$ crosses the depth z_A at angles spanning the angular sector $\left[\arccos\frac{c_A}{c_0}, \arccos\frac{c_A}{c_S}\right]$, which is narrower than

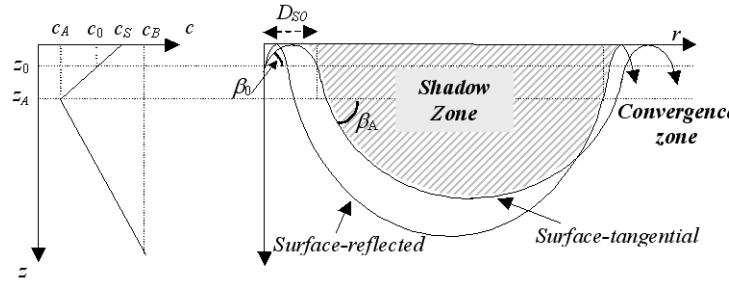

Figure 2.30 Shadow-zone geometry. The ray transmitted at angle β_0 is just grazing at the surface. All steeper rays hit the surface, and are then deflected downward before the surface-tangent ray. No direct path can penetrate inside the shadow zone limited by the surface-tangential ray.

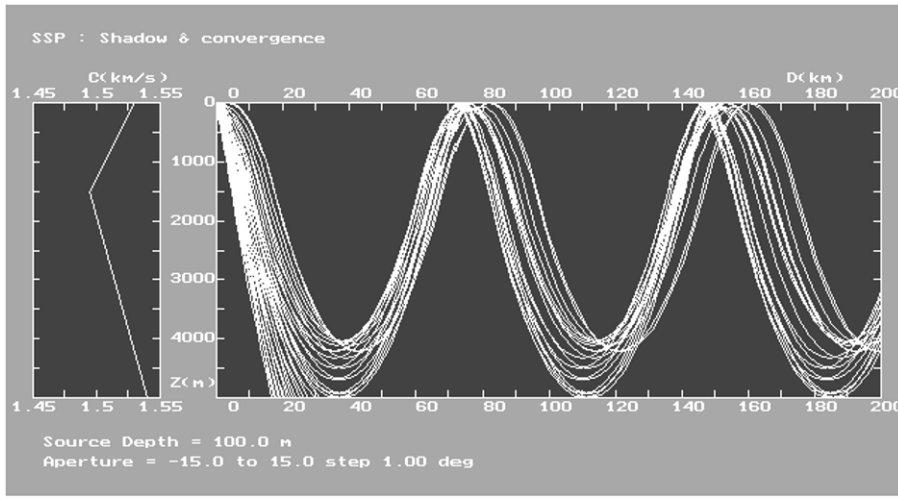

Figure 2.31 Propagation in a deep channel: shadow and convergence zones, with a shallow source. The narrowness of the ray bundle depends on the source depth.

the transmitted sector. These grouped rays all follow approximately the same refracted geometrical path, and therefore they undergo a very small divergence spreading. The same ray bundle can be followed after its refraction by the deep gradient, still concentrated in a *convergence zone* (or *resurgence zone*), insonified very favorably (Figure 2.31). The empty space left by this ray concentration is called a *shadow zone*, which cannot be insonified directly from the source (at least in the strict frame of ray tracing modeling, since diffraction outside geometrical beams becomes noticeable at very low frequencies). Indirect insonification through bottom bounce remains possible, of course, but affected by reflection losses. All considered, a shadow zone is therefore unfavorable energetically.

The convergent beam bundle then propagates further with the same cyclic characteristics. The convergence zone is duplicated along range, somewhat widening with propagation, and becoming increasingly blurred (Figure 2.31). The size of shadow zones and the periodicity of convergence zones depend on the general sound speed profile (typically 40 km in the Mediterranean, 60 km in the Atlantic).

This type of configuration is very important in ASW tactics in deep water, where submersibles and sonars move at relatively shallow depths. The shadow zones are used to hide, and the convergence zones are favored places for detection.

2.9 WAVE CALCULATIONS OF THE ACOUSTIC FIELD

Wave techniques aim at giving a complete solution for the complex acoustic field. They are based on the direct solution, through different techniques, of the propagation equation.

Typically, these techniques are required when the acoustic field is to be described with a resolution close to the wavelength, so that its wave behavior can be analyzed with high enough accuracy. They are therefore mostly used for very low frequencies[19], where the oscillations/interferences of the field are stable enough to be practically observable. The geometric approach is preferred at high frequencies, where it is more suitable and numerically faster.

Wave solutions are also better designed for monochromatic signals, and are less suited to the description of transitory signals. They will therefore be useful in the application context of low-frequency permanent narrowband signals (e.g., ship-noise propagation and passive sonars), or the very accurate description of active low-frequency signals when ray modeling becomes dubious. Geometric approaches, well-adapted to transitory processes (travel times), should therefore be usually preferred for active detection/measurement applications.

An important constraint in the wave propagation modeling is the kind of spatial variability of the medium that has to be taken into account. We have seen in Section 2.6 that the main variations of sound velocity are in the depth direction. When only these variations are considered and when the ocean bottom is flat and horizontal, the medium is said to be stratified. This yields considerable mathematical simplification. When the wave path encounters mesoscale structures like fronts or eddies, as it may occur in long range propagation, or when the topography of the bottom has to be accounted for, as in some shallow water configurations, the medium has to be considered non-stratified, the propagation modeling complexity increases and computation cost increases.

The following description of wave techniques is far less detailed than the complexity of the subject ought to warrant. Once again, the reader is sent to the more specialized works by Tolstoy and Clay (1987), Brekhovskikh and Lysanov (1992), and Jensen *et al.* (1994).

2.9.1 Modal method

2.9.1.1 Stratified waveguide

This method starts from the propagation equation for a stratified medium, with sound velocity $c(z)$ (or wave number $k(z)$), and a point source at depth z_0 ($r = 0$):

$$\Delta p(r, z, z_0) + k^2(z) p(r, z, z_0) = -\frac{2}{r}\,\delta(r)\delta(z - z_0) \tag{2.92}$$

The source term in (2.92) is equivalent to $-4\pi\delta(x)\delta(y)\delta(z)$ in Cartesian coordinates, so that the near field behaves like a spherical source of unit amplitude $\exp(jkR)/R$. By cylindrical symmetry, a two-dimensional solution $p(r, z)$ of the Helmholtz equation can be separated into a function Γ depending on r only, and a function Φ depending on z only:

$$p(r, z) = \Gamma(r)\Psi(z) \tag{2.93}$$

[19] Here, the notion of high or low frequencies is also relative to the height of the waveguide, in ratio to the acoustical wavelength.

We introduce a constant K^2 separating the variables in the propagation equation expressed in cylindrical coordinates:

$$\begin{cases} \dfrac{d^2\Gamma}{dr^2} + \dfrac{1}{r}\dfrac{d\Gamma}{dr} + K^2\Gamma = -\dfrac{2}{r}\,\delta(r) \\ \dfrac{d^2\Phi}{dz^2} + (k^2(z) - K^2)\Phi = 0 \end{cases} \tag{2.94}$$

The first equation is a *Bessel equation*. For a wave spreading from the source, its outgoing solution is proportional to the Hankel function of the first kind[20] (Abramowitz and Stegun, 1964):

$$\Gamma(r) = j\pi H_0^{(1)}(Kr) \tag{2.95}$$

For large values of its argument (in fact as soon as it is greater than 1), this function tends toward the asymptotic expression:

$$H_0^{(1)}(x) \to \sqrt{\frac{2}{\pi x}}\exp\left[j\left(x - \frac{\pi}{4}\right)\right] \tag{2.96}$$

The second equation of (2.94), with z-dependence, must be verified simultaneously with the continuity conditions at the waveguide boundaries:

- the pressure at the air-water interface is null: $\Phi(0) = 0$
- the condition at the water-bottom interface is of the general form $F\left\{\Phi(H), \dfrac{d\Phi}{dz}(H)\right\} = 0$ (e.g.: $\dfrac{d\Phi}{dz}(H) = 0$ for a perfectly rigid seafloor).

The differential equation in z associated with these conditions has a series of solutions expressed as $\{K = k_n, \Phi(z) = \Phi_n(z)\}$, for $n = 1, 2, \ldots N$. These are called *propagation eigenmodes*. Each mode verifies the following system of equations:

$$\begin{cases} \dfrac{d^2\Phi_n}{dz^2} + (k^2(z) - k_n^2)\Phi_n = 0 \\ \Phi_n(0) = 0 \\ F\left\{\Phi_n(H), \dfrac{d\Phi_n}{dz}(H)\right\} = 0 \\ \displaystyle\int_0^H \Phi_n(z)\Phi_m(z)\,dz = \delta_{mn} \end{cases} \tag{2.97}$$

The latter equation (where δ_{mn} is the Kronecker symbol) corresponds to the *orthonormality* of the eigenmodes[21]. Using this property and the asymptotic

[20] Note that in this section, the harmonic time dependence of the pressure is $\exp(-j\omega t)$, according to the main part of the literature on the subject.

[21] For $n = m$, the normalization expression is exact only for perfectly reflecting boundaries. For a general boundary condition, an additional term is needed, corresponding to the integration from H to ∞.

expression (2.96) of the Hankel function, the solution of (2.92) for the far field can finally be expressed as:

$$p(r,z,z_0) = \sqrt{\frac{2\pi}{r}} \sum_n \frac{\Phi_n(z)\Phi_n(z_0)}{\sqrt{k_n}} \exp\left[j\left(k_n r + \frac{\pi}{4}\right)\right] \tag{2.98}$$

Under this form, the modal field is consistent with the field radiated by a spherical source of unit amplitude; in other words, Expression (2.98) gives the transmission loss relatively to a reference point at unit distance from the source.

The main difficulty of this method therefore consists in determining the wave numbers $\{k_n\}$ of the eigenmodes (and thus the corresponding wave functions). In the simple case where the sound velocity is constant (see Appendix A.2.3), the wave functions are trigonometric functions that are easily calculable, of type $\Phi_n(z) \propto \sin(\sqrt{k^2 - k_n^2}\, z)$. The eigenmodes are to be separated in two categories:

- the *propagating modes*, whose wave numbers k_n are real, and which carry most of the acoustic field energy;
- the *attenuated modes*, with complex wave numbers, whose contribution is noticeable only at short ranges from the source.

An example of application is given in Figure 2.32, showing the wave functions of the 24 first modes (propagating and attenuated), and the resulting field. The latter is to be compared with Figure 2.10, which was obtained geometrically for the same configuration.

The total number of modes (propagating and attenuated) N_m is approximately given by the ratio of the water depth to the average half-wavelength for the frequency considered (see (A.2.3.6) in Section A.2.3.1):

$$N_m \approx \frac{2H}{\lambda} \tag{2.99}$$

It is therefore proportional to the frequency. This number of modes is an interesting indicator of the applicability of the modal technique. A number of a few tens is optimal (Figure 2.32). Beyond a few hundreds, the use of geometric acoustics is undoubtedly justified. Conversely, if the number of modes is too small, a method of direct numerical integration (see Section 2.9.2) is preferable.

To understand this modal description more physically (Brekhovskikh and Lysanov, 1992) for a constant velocity profile, one reads;

$$\sin k_z z = \frac{\exp(jk_z z) - \exp(-jk_j z)}{2j}$$

that is, the wave function is considered as the sum of an up-going wave and a down-going wave interfering in the waveguide. Thus:

- the existence of an eigenmode corresponds to a plane wave constructively interfering with itself after reflections at the interfaces;
- the propagating modes correspond to total reflection on the bottom, at over-critical incidence.
- the attenuated (or leaky) modes correspond to energy loss by reflection on the bottom, at sub-critical incidence.

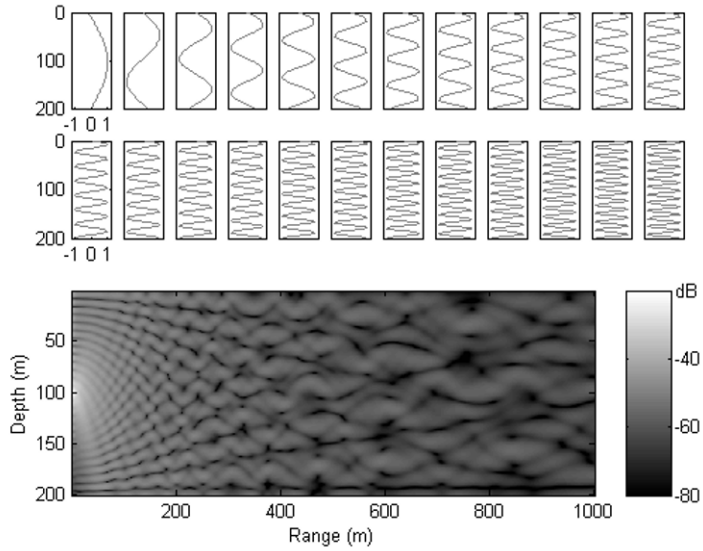

Figure 2.32 Normal-mode depth functions $\Phi_n(z)$ (amplitudes normalized to unity) in a constant-velocity channel at 100 Hz, with the first 24 modal waveforms (top), and resulting pressure field in dB (bottom). For comparison, the configuration is the same as in Figure 2.10.

For real sound speed profiles $c(z)$, the wave functions have no closed-form expression, as in the isovelocity case, except for a few specific profiles. The problem can then be solved in two ways: either by splitting the sound velocity profile into sections which each admit a closed-form expression, like *Airy functions* for linear squared wave-number, and forcing continuity conditions between the layers; or by numerically solving the whole differential equation in z with its boundary conditions.

2.9.1.2 Non-stratified waveguide

The method of eigenmodes, physically based on vertical resonances of the water column, is by its very nature linked to a *stratified waveguide structure*. However, it can be extended to media with a range dependence. The basic principle of these extensions is to consider the modal structure as a local notion, either discrete (the medium is divided, along horizontal extent, into discontinuous stratified sections in which one calculates the eigenmodes), or continuous. The problem then lies in joining the modal series obtained locally. Two methods can be used:

- The method of *coupled modes* consists in imposing continuity conditions between the sections of the horizontally-gridded medium, over the entire vertical field structure. These conditions lead to coupling coefficients between the modes determined inside the different sections. This method is theoretically rigorous, but quite heavy computationally.

- The method of *adiabatic modes* is lighter numerically and more interesting physically. Assuming the medium varies slightly with range, this method assumes that each mode transforms with no energy loss into the corresponding mode (of the same order) in the neighboring section. This implies that the transitions between sections are quite progressive, and this limits the calculation of the number of modes to its minimum local value (i.e., at the smallest water depth). This adiabatic mode method is frequently used, because of its relative simplicity.

For modeling propagation in non-stratified media, modal methods are nowadays most often replaced by the parabolic equation technique (see Section 2.9.3).

2.9.2 Complete solution of the wave equation in stratified media

The method of the preceding section somewhat "forces" the modal nature of the pressure field. We will briefly see in this section that additional components may be brought out and computed.

2.9.2.1 Integral formulation of the field

Because of the cylindrical symmetry induced by a point source in a stratified medium, the general solution to equation (2.92) can be written as the integral of the contributions from a spectrum of cylindrical waves characterized by the horizontal component k_r of their wave number, namely a Fourier-Bessel integral:

$$\begin{aligned} p(r, z, z_0) &= \int_0^{\infty} G(k_r, z, z_0) J_0(k_r r) k_r dk_r \\ &= \frac{1}{2} \int_{-\infty}^{+\infty} G(k_r, z, z_0) H_0^1(k_r r) k_r dk_r \end{aligned} \tag{2.100}$$

where J_0 is the Bessel function of 0^{th} order and H_0^1 is the Hankel function of the first type and 0^{th} order. G is the one-dimension *Green function* of the medium, obeying the following conditions:

- one-dimensional ordinary differential equation in z, parameterized by k_r;
- boundary conditions at the surface and the bottom;
- source conditions at $z = z_0$: continuity of G and discontinuity of $\dfrac{dG}{dz}$.

The system to be solved is similar to the system with wave functions of the *eigenmodes*, with the addition of the source conditions. Two methods can be used to evaluate the integral over the real wavenumber axis in Equation (2.100).

The first one is analytical and consists in closing the integration contour in the complex plane (Ahluwalia and Keller, 1977). Two kinds of terms contribute to the integral:

- The *residues* associated to the *poles* of the one-dimension Green function. These discrete contributions correspond to the eigenmodes presented in the previous section. Poles on the real axis correspond to propagating modes and poles with non-zero imaginary parts correspond to leaky modes.
- A *branch-line integral*. For example in the case of a fluid bottom, the interface impedance (or the reflection coefficient) involves a square root of the difference between the squared wave number in the bottom and the squared horizontal wave number k_r in the fluid (see Appendix A.2.3.2). Hence a branch cut is necessarily introduced in the complex plane. The associated branch line integral corresponds to the refracted wave that is incident on the bottom at the critical angle, propagates along the interface with the sound speed of the bottom, and continuously radiates toward the water at critical angle. Such waves arise for different types of bottom conditions. Because of the radiation, the geometrical spreading of these waves is greater than cylindrical (amplitude varying in $1/r^a$ with $a > 1/2$), their contribution in the far field is weak and they may be observed only if they are time-resolved; see (Brekhovskikh and Godin, 1999) for an expanded presentation of this *lateral wave*. Note that this phenomenon is exploited in geophysics; it is known as *refracted wave* in the seismic propagation terminology (see Section 9.3.2.8), and is used because of its capability to provide the velocity value in the underlying layer.

A second method for evaluating Equation (2.100) is a numerical integration, and is the subject of the following paragraph.

2.9.2.2. Numerical solution

Numerical computation of the integral (2.100) over the spectrum in k_r is made easier if the Hankel function is approximated by its asymptotic form (2.96). This allows writing $p(r, z)$ as:

$$p(r, z, z_0) \approx \sqrt{\frac{1}{2\pi r}} \int_{-\infty}^{+\infty} G(k_r, z, z_0) \sqrt{k_r} \exp(j(k_n r - \pi/4)) dk_r \qquad (2.101)$$

This is in fact a Fourier transform, which can be computed with FFT algorithms[22]. The main part of the calculation thus consists in the evaluation of $G(z, z_0, k)$ for a series of values sampling the domain $\{k_r\}$ of interest. The FFT results in a series of values of p as a function of range, for a given couple (z, z_0).

The fundamentals of this method (described in, e.g., Jensen *et al.*, 1994) date back to the 1970s. Its main interest is to provide a very accurate reference solution in the case of a stratified medium. Its main defect is that it does not give a direct access to the physical interpretation of the problem. It is mostly used as a benchmark for calculations of the propagation of very-low frequency monochromatic signals, or their reflection, in stratified media. Beyond this reference role, its practical utility for operational applications is limited.

[22] The method was originally known as FFP, for *Fast Field Program*.

2.9.3 Parabolic equation method

In this section, we consider low- to mid-frequency propagation in a range-dependent ocean, encountered when oceanic features like eddies, thermal fronts, or simply the bottom topography have to be taken into account.

The *parabolic equation method* is generally suited to the description of wave propagation in inhomogeneous media where a preferred direction of propagation exists, as in natural or artificial waveguides, or for the propagation of narrow beams in inhomogeneous unbounded media. This implies that the environment does not vary too fast with range and azimuth, which is generally the case in underwater acoustics. The equation to be solved is the (elliptic) Helmholtz equation that is second order in range and has then to be solved globally (if the medium is not stratified), for example using finite elements methods with appropriate boundary conditions. For propagation ranges and frequencies of practical interest, this often leads to prohibitive computational loads and memory requirements.

The method first consists in separating the global pressure field into forward and backward propagating waves, with respect to the preferred direction that we consider horizontal, and in the *decoupling* of these waves. Secondly, the resulting equation for the forward propagating wave involves a square-root operator that implies a *paraxial approximation* to be made explicit.

Being first-order in range, the parabolic, or more generally one-way, wave equation can be numerically integrated step by step from the source.

2.9.3.1 Separation of forward and backward propagating waves

This method is used for environments slowly varying with range and azimuth. In the case of a three-dimensional depth-velocity profile $c(x, y, z)$, the local wavenumber may be expressed as:

$$k(x, y, z) = k_0 n(x, y, z) = k_0 \frac{c_0}{c(x, y, z)} \tag{2.102}$$

where c_0 is a reference velocity of the medium and k_0 the corresponding wave number. The Helmholtz equation reads, apart from the source:

$$\Delta p + k_0^2 n^2(x, y, z) p = 0. \tag{2.103}$$

In cylindrical coordinates (r, θ, z), with the vertical axis passing through the source, this equation reads:

$$\frac{1}{r}\frac{\partial}{\partial r}\left(r\frac{\partial p}{\partial r}\right) + \frac{1}{r^2}\frac{\partial^2 p}{\partial \theta^2} + \frac{\partial^2 p}{\partial z^2} + k_0^2 n^2(r, \theta, z) p = 0. \tag{2.104}$$

Most frequently, the horizontal variations of the sound velocity are weak, so that horizontal refraction can be neglected. The acoustical energy initially present in a vertical plane containing the source will thoroughly stay in that plane. Dropping the

second term in the left-hand side of Equation (2.104), we obtain, in a vertical plane, the two-dimensional wave equation:

$$\frac{1}{r}\frac{\partial}{\partial r}\left(r\frac{\partial p}{\partial r}\right)+\frac{\partial^2 p}{\partial z^2}+k_0^2 n^2(r,\theta,z)p=0. \tag{2.105}$$

This approximation is commonly referred to as the $N\times 2\mathrm{D}$ approximation, the approximation being repeated in N vertical planes ($\theta=\theta_n, n=1,N$).

It is then convenient to account for the cylindrical spreading by considering the following change of variable:

$$p=\frac{\varphi}{r^{1/2}}. \tag{2.106}$$

Inserting this expression into Equation (2.105) gives, dropping the parameter θ:

$$\frac{\partial^2\varphi}{\partial r^2}+\frac{\varphi}{4r^2}+\frac{\partial^2\varphi}{\partial z^2}+k_0^2 n^2(r,z)\varphi=0, \tag{2.107}$$

so that, sufficiently far from the source, the second term of the left-hand side of this equation may be neglected, and the reduced field φ satisfies a standard bi-dimensional Helmholtz equation:

$$\frac{\partial^2\varphi}{\partial r^2}+\frac{\partial^2\varphi}{\partial z^2}+k_0^2 n^2(r,z)\varphi=0 \tag{2.108}$$

Let us write this latter equation in a form that highlights the global propagation along the r direction:

$$\frac{\partial^2\varphi}{\partial r^2}+k_0^2 Q\varphi=0, \tag{2.109}$$

where Q is a differential operator acting on functions of z, and parametrically depending on r:

$$Q(r)=\frac{1}{k_0^2}\frac{\partial^2}{\partial z^2}+n^2(r,z). \tag{2.110}$$

The propagation equation (2.108) then reads:

$$\left(\frac{\partial}{\partial r}+jk_0Q^{1/2}\right)\left(\frac{\partial}{\partial r}-jk_0Q^{1/2}\right)\varphi+jk_0\frac{\partial Q^{1/2}}{\partial r}\varphi=0. \tag{2.111}$$

If the medium is stratified, the index n and then the operator Q do not depend on r, so that the last term in the left-hand side of Equation (2.111) cancels, providing the exact factorization:

$$\frac{\partial}{\partial r}\varphi=\pm jk_0Q^{1/2}\varphi. \tag{2.112}$$

When the medium is not stratified but slowly varies with range, one still considers this factorization but reintroducing the dependence of operator Q on r:

$$\frac{\partial}{\partial r}\varphi = \pm jk_0 Q(r)^{1/2}\varphi. \tag{2.113}$$

With the convention of a temporal term $\exp(-j\omega t)$, the + sign corresponds to waves outgoing from the source, while the minus sign corresponds to incoming waves.

2.9.3.2 The paraxial approximation

Up to this point the derivation is somewhat formal since the square root of the operator Q given by the definition (2.110) is an unknown pseudo-differential operator. Explicit local approximations of this operator may be obtained by using the paraxial approximation. For a plane wave in a medium of sound speed c_0, the first term in the right-hand side of definition (2.110) represents the squared sine of the grazing propagation angle, which is small for long-range propagation. In an inhomogeneous ocean, relative variations of the sound speed remain small and the index is close to 1. As a consequence, waves propagating with low grazing angles will continue to do so. It is then appealing to write the operator Q under the form

$$Q(r) = 1 + \varepsilon, \tag{2.114}$$

$$\text{with} \quad \varepsilon = \frac{1}{k_0^2}\frac{\partial^2}{\partial z^2} + n^2(r,z) - 1 \tag{2.115}$$

In the far field, waves propagating with high grazing angles have been most attenuated due to successive interaction with the bottom, so that the norm of operator ε is small, authorizing explicit approximation for the square root operator appearing in equation (2.113).

The first-order Taylor approximation reads

$$(Q(r))^{1/2} \approx 1 + \frac{\varepsilon}{2}. \tag{2.116}$$

Inserting this expression into Equation (2.113) leads to the standard parabolic equation for outgoing waves:

$$\frac{\partial}{\partial r}\varphi = \frac{jk_0}{2}(1 + n^2)\varphi + \frac{j}{2k_0}\frac{\partial^2\varphi}{\partial z^2} \tag{2.117}$$

This equation was first introduced in the 1940s by Fock and Leontovitch in the context of electromagnetic waves and in the 1970s by Tappert in underwater acoustics, and is formally equivalent to the time-dependent Schrödinger equation (with range playing the role of time). It is often referred to as the "small angle" parabolic equation, and is generally considered to give good results in underwater acoustics for waves up to grazing angles of 15°.

Due to this latter limitation, the standard parabolic equation is now rarely used. More accurate approximation are preferred, and particularly the Padé, or rational,

one. The simplest non-trivial approximation has been introduced by Claerbout in the 1970s in the context of seismic waves:

$$(Q(r))^{1/2} \approx \frac{1+\frac{3}{4}\varepsilon}{1+\frac{1}{4}\varepsilon}, \tag{2.118}$$

yielding the propagation equation

$$\left(1+\frac{1}{4}\varepsilon\right)\frac{\partial}{\partial r}\varphi = jk_0\left(1+\frac{3}{4}\varepsilon\right)\varphi, \tag{2.119}$$

with ε given by (2.115). This equation has been considered as giving reasonably good results for grazing angles up to 40°.

Generalized Padé approximants are of the form:

$$(Q(r))^{1/2} \approx 1+\sum_{i=1}^{n_p}\frac{a_i\varepsilon}{1+b_i\varepsilon} \quad \text{with} \begin{cases} a_i = \dfrac{2}{2n_p+1}\sin^2\left(\dfrac{i\pi}{2n_p+1}\right) \\ b_i = \cos^2\left(\dfrac{i\pi}{2n_p+1}\right) \end{cases} \tag{2.120}$$

It has to be noticed that these approximated square-root operators have the same *eigenvectors* as the exact one but with approximated *eigenvalues*. As a consequence,

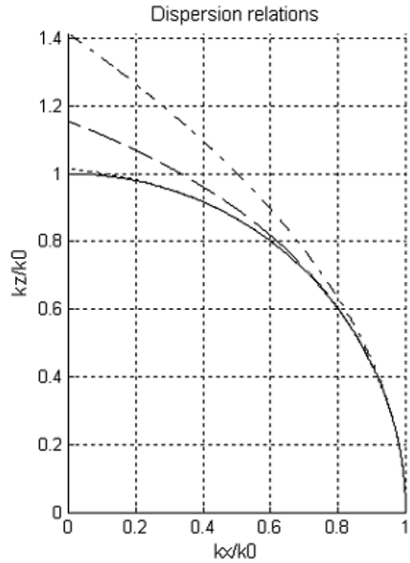

Figure 2.33 Dispersion relation in an homogeneous ocean for different approximations of the square-root operator. - : exact (Helmholtz equation); -. : first order Taylor series (small angle equation 2.116); – – : Padé approximation, $n_p = 1$ (Claerbout equation 2.118), ... : Padé approximation equation 2.120, $n_p = 4$.

the exact modes will be correctly propagated with regard to amplitude (i.e. without spurious coupling) but with approximated phases (see, for example, Equation (2.98)).

The effect of these different approximations on the relation between vertical and horizontal wave numbers in an homogeneous ocean are presented in Figure 2.33, along with the exact solution $k_x = (k_0^2 - k_z^2)^{1/2}$. As expected, larger errors on k_x, and thus on phases, will occur at high angles (large k_z) but the convergence of Padé expansions is very fast so that very high angle propagation equations are obtained with few terms in the expansion.

2.9.3.3 Further developments – implementation

It has long been recognized that the one-way wave equation (2.113) does not always give the correct amplitude of the field for severe range dependence (Collins and Westwood (1991), Porter (1991), Godin (1999)). Various corrections have been proposed in particular in order to ensure conservation of energy flux, without this constraint being theoretically justified. In fact the passage from (2.111) to (2.113) is questionable. The proper way to derive the one-way wave equation is to consider the first term of a Bremmer series (see for example Brekhovskikh and Godin, 1998, for an introduction in one dimension). This approach leads, instead of (2.112), to the one-way wave equation:

$$\frac{\partial}{\partial r}\varphi = (\pm jk_0 Q^{1/2} - \tfrac{1}{2} Q^{-1/2} Q_x^{1/2})\varphi, \tag{2.121}$$

where $Q_x^{1/2}$ is the range derivative of operator $Q^{1/2}$. It is then shown that energy conservation is only ensured in a high frequency limit, relatively to the range dependence of the medium (Leviandier, 2009).

The main interest of the parabolic, or one-way, equation is that it is first-order in range. Thus it can be solved step by step, the outgoing radiation condition being *de facto* satisfied. The usual way to numerically solve this equation is:

- to calculate the field $\varphi(r_0, z)$ at an initial range r_0 by another technique (modes, rays, Gaussian field, etc.);
- to continue with r beyond r_0 with a numerical technique, e.g., finite differences and alternating direction implicit method for the Padé approximation.

The above scheme requires to grid the vertical plane with a sub-wavelength step in both the vertical and horizontal directions. The constraint in the horizontal direction may be relaxed to a certain extent in slowly range-dependent ocean by considering an approximation of the propagating operator itself (rather than its infinitesimal generator):

$$\varphi(r + \Delta r, z) \approx e^{jk_0 \Delta r Q(r)^{1/2}} \varphi(r, z) \approx \left(1 + \sum_{i=1}^{n_p} \frac{a_i' \varepsilon}{1 + b_i' \varepsilon}\right) \varphi(r, z) \tag{2.122}$$

The technique, known as the split-step Padé method (Collins, 1993), authorizes integration steps largely greater than the wavelength for a slowly range-dependent ocean, so reducing significantly the computation time.

More detailed presentations of the parabolic approximation method are to be found in e.g. (Jensen, 1994) or (Lee, 2000). This method is currently the most used to investigate low frequency propagation in non-stratified media. Its routine use at mid-frequency or for full three-dimensional configuration is still limited by computation load.

http://www.springer.com/978-3-540-78480-7

An Introduction to Underwater Acoustics
Principles and Applications
Lurton, X.
2010, XXXVI, 724 p. 32 illus. in color., Hardcover
ISBN: 978-3-540-78480-7